Metabolic and immunomodulatory effects of n-3 fatty acids are different in mesenteric and epididymal adipose tissue of diet-induced obese mice

Tobias Ludwig,^{1,3} Stefanie Worsch,^{1,3} Mathias Heikenwalder,⁴ Hannelore Daniel,² Hans Hauner,^{1,3} and Bernhard L. Bader^{1,3}

¹Clinical Nutritional Medicine Unit, ZIEL-Research Center for Nutrition and Food Sciences, Technische Universität München, Freising-Weihenstephan, Germany; ²Biochemistry Unit, ZIEL-Research Center for Nutrition and Food Sciences, Technische Universität München, Freising-Weihenstephan, Germany; ³Else Kröner-Fresenius-Centre for Nutritional Medicine, Technische Universität München, Freising-Weihenstephan, Germany; and ⁴Institute of Virology, Technische Universität München und Helmholtz-Zentrum München, Munich, Germany

Submitted 5 April 2012; accepted in final form 8 March 2013

Ludwig T, Worsch S, Heikenwalder M, Daniel H, Hauner H, Bader BL. Metabolic and immunomodulatory effects of n-3 fatty acids are different in mesenteric and epididymal adipose tissue of diet-induced obese mice. Am J Physiol Endocrinol Metab 304: E1140-E1156, 2013. First published March 12, 2013; doi:10.1152/ajpendo.00171.2012.—In studies emphasizing antiobesogenic and anti-inflammatory effects of long-chain n-3 polyunsaturated fatty acids (LC-n-3 PUFA), diets with very high fat content, not well-defined fat quality, and extreme n-6/n-3 PUFA ratios have been applied frequently. Additionally, comparative analyses of visceral adipose tissues (VAT) were neglected. Considering the link of visceral obesity to insulin resistance or inflammatory bowel diseases, we hypothesized that VAT, especially mesenteric adipose tissue (MAT), may exhibit differential responsiveness to diets through modulation of metabolic and inflammatory processes. Here, we aimed to assess dietary LC-n-3 PUFA effects on MAT and epididymal adipose tissue (EAT) and on MAT-adjacent liver and intestine in diet-induced obese mice fed defined soybean/palm oilbased diets. High-fat (HF) and LC-n-3 PUFA-enriched high-fat diet (HF/n-3) contained moderately high fat with unbalanced and balanced n-6/n-3 PUFA ratios, respectively. Body composition/organ analyses, glucose tolerance test, measurements of insulin, lipids, mRNA and protein expression, and immunohistochemistry were applied. Compared with HF, HF/n-3 mice showed reduced fat mass, smaller adipocytes in MAT than EAT, improved insulin level, and lower hepatic triacylglycerol and plasma NEFA levels, consistent with liver and brown fat gene expression. Gene expression arrays pointed to immune cell activation in MAT and alleviation of intestinal endothelial cell activation. Validations demonstrated simultaneously upregulated pro- (TNFα, MCP-1) and anti-inflammatory (IL-10) cytokines and M1/M2-macrophage markers in VAT and reduced CD4/CD8α expression in MAT and spleen. Our data revealed differential responsiveness to diets for VAT through preferentially metabolic alterations in MAT and inflammatory processes in EAT. LC-n-3 PUFA effects were pro- and anti-inflammatory and disclose T cell-immunosuppressive potential.

obesity; mesenteric adipose tissue; metabolism; inflammation; macrophages

obesity has become a major health problem and is associated with the metabolic syndrome, cardiovascular diseases, type 2 diabetes, development of inflammatory bowel diseases, and colon cancer (6, 24, 60). Excessive abdominal fat, such as omental and mesenteric adipose tissue (MAT), has been asso-

ciated with insulin resistance and cardiovascular diseases (23. 40, 74). Moreover, visceral adipose tissues (VAT) differ in cellular composition and molecular properties from subcutaneous adipose tissue by enhanced secretion of proinflammatory factors (5). MAT may directly influence liver metabolism by secretion of free fatty acids and adipokines into the portal vein, leading to hepatic production of inflammatory cytokines, coagulation factors, and hepatic lipid accumulation and finally to hepatic insulin resistance, type 2 diabetes, and nonalcoholic fatty liver disease. MAT covers mesenteric lymph nodes (MLN) and mesenteric vasculature that supplies the intestine with blood and lymphatic vessels that drain into the portal vein and MLN/collecting lymph trunk, respectively. Thus, the mesenteric, intestinal and portal blood, and intestinal functions for nutrient absorption and as immune organ establish the connectivity between MAT/MLN, intestine, and liver.

Diet-induced obesity (DIO) models in mice usually employ high-fat diets that cause excessive adipose tissue development and lead to impairments in lipid and glucose metabolism, ultimately leading to insulin resistance (4, 22). n-6 Polyunsaturated fatty acids (PUFA), being abundant in the Western diet, can increase inflammatory signals and have been associated with adipose tissue expansion and cardiovascular heart disease. Dietary constituents that may counteract these impairments and the metabolic syndrome are the PUFA of the n-3 class. However, n-6 PUFA are more abundant in the Western diet than n-3 PUFA, which can apparently generate a molecular competition between n-6 PUFA and n-3 PUFA for several physiological processes (1, 63, 64, 73). For long-chain n-3 (LC-n-3) PUFA, positive effects on insulin secretion are described, although effects on glucose tolerance are not consistent (14). Furthermore, lipid-lowering effects in high-fat diet-induced hypertriglyceridemia have been reported in various intervention studies (29, 30).

There are functional differences between different adipose tissue depots. VATs contribute more to the obesity-related complications than other fat depots (23, 40, 74), but the differential VAT responsiveness to specific diet composition has rarely been studied in DIO mouse models (5, 7, 16). In rodent studies, epididymal adipose tissue (EAT) is most frequently used as representative of VAT because it is easily accessible. However, it does not necessarily compare with visceral fat depots in human anatomy. Therefore, intra-abdominal MAT, which is anatomically comparable in mice and humans, may present a more suitable depot for comparative analysis of adipose tissue impairments in obesity. Compared

Address for reprint requests and other correspondence: B. L. Bader, Technische Universität München, ZIEL, Nutritional Medicine Unit, Gregor-Mendel-Strasse 2, 85350 Freising-Weihenstephan, Germany (e-mail: bernhard.bader@tum.de).

with other fat depots, MAT shows apparently functional differences in gene expression and higher metabolic activity, and it has been implicated in the development of metabolic syndrome and inflammatory bowel diseases (5, 51, 60, 74). For example, creeping fat in patients with Crohn's disease refers to hypertrophy of MAT located around the inflamed intestine, and only a few studies have addressed the contribution of MAT in the development of insulin resistance (7, 16).

Obesity is associated with a chronic inflammatory state in adipose tissue leading to immune cell infiltration and recruitment as well as macrophage differentiation and activation. Macrophages and T cells and, as recently discovered, also B cells, can infiltrate the fat depots as they expand (33, 46, 55, 77, 79), and adipokines secreted by adipocytes may serve as attractants (24). In an obese state, adipocytes show hypertrophy and an imbalance between cell proliferation and apoptosis, and it has been proposed that adipose tissue macrophages (ATM), which are usually of an anti-inflammatory M2 macrophage phenotype, undergo a phenotypic switch to a more proinflammatory M1 macrophage phenotype (37, 38). M1 macrophages are recruited predominantly to localize around dead adipocytes, forming necrotic crown-like structures (CLS), but M1 macrophages can also be recruited to accumulated cell clusters of active remodeling, where M2 macrophages are more abundant (10, 38, 67). In rodent DIO models, diets containing up to 60% energy derived from fat are employed. However, it is also known that different fatty acids modulate obesity-related complications differentially in terms of the development of insulin resistance and type 2 diabetes (4, 14). Moreover, extreme ratios of LC-n-6 PUFA (e.g., arachidonic acid) to LC-n-3 PUFA [e.g., eicosapentaenoic acid (EPA) and docosahexaenoic acid (DHA)] of up to 200:1 have been used (26), whereas human diets have more balanced n-6 PUFA/n-3 PUFA ratios of 17:1 to 1:1 (63). In contrast to LC-n-6 PUFA, it has been reported frequently that LC-n-3 PUFA exert anti-inflammatory actions in the context of cardiovascular diseases and adipose tissue inflammation and seem to possess antiadipogenic effects (57). Mechanisms underlying these LC-PUFA functions include 1) the modification of membrane composition by LC-PUFA containing phospholipids, which affects membrane fluidity, transport functions, and signaling processes, 2) changes in gene expression, and 3) effects in response to their specific metabolites acting as lipid mediators (1, 62, 64, 73).

In the present study, we induced obesity in male C57BL/6J mice by feeding defined soybean/palm oil-based diets [control (C), isocaloric high-fat (HF), and LC-n-3 PUFA-enriched HF diet (HF/n-3)] for 12 wk. Diets were characterized by low fat content (13 kJ% fat) for the control diet, moderately high-fat content (48 kJ% fat) for the isocaloric high-fat diets, and unbalanced (C, 9.85:1; HF, 13.5:1) and balanced (HF/n-3, 1:0.84) n-6/n-3 PUFA ratio. First, we performed a basic metabolic characterization of obese and lean control mice. Then, we examined the differential responsiveness to diets for VAT by analyzing metabolic and immunomodulatory processes in MAT and EAT. As a consequence of the observed antiobesogenic and potentially both immunoenhancing and immunosuppressive effects of LC-n-3 PUFA in VAT, we complemented our study in mice by analyzing metabolic and immunological aspects in the MAT-adjacent liver and intestine as well as in brown adipose tissue (BAT) and spleen.

EXPERIMENTAL PROCEDURES

Mice and diets. Six-week-old male C57BL/6J mice were obtained from Charles River Laboratories (Sulzfeld, Germany) and singlehoused under controlled, specific, pathogen-free conditions at 22°C and 50-60% humidity with a 12:12-h light-dark cycle. Animals had ad libitum access to food and water. All diets were purified experimental diets manufactured as pellets by Ssniff Spezialdiäten (Soest, Germany), followed by 25 kGy/min γ-radiation (Isotron Deutschland, Allershausen, Germany), and stored in the dark at -20° C (long term) and 4°C (short term). For the 12-wk feeding trial, mice were first fed a control diet for 2 wk, and at the age of 8 wk, animals were randomly assigned to three dietary groups (n = 12 mice/group): control diet with 13 kJ% fat (C; cat. no. S5745-E720), high-fat diet with 48 kJ% fat (HF; cat. no. S5745-E722), and high-fat diet enriched with a LC-n-3 PUFA concentrate (EPAX 1050-TG; rich in EPA and DHA, kindly provided by Goerlich Pharma International, Edling, Germany) with 48 kJ% fat (HF/n-3; cat. no. S5745-E725). Detailed diet compositions and metabolizable energy of diets (provided in Table 1) were constant among diets for the following ingredients (in wt/wt): 24% casein, 5.6% maltodextrin, 5% sucrose, 5% cellulose, 1.2% vitamins, and 6% minerals. Fat and starch content were the only variables (C: 5% soybean oil and 47.8% corn starch; HF: 5% soybean oil, 20% palm oil, and 27.8% corn starch; HF/n-3: 5% soybean oil, 11.25% palm oil, 8.75% EPAX 1050 TG, and 27.8% corn starch). All diets were supplemented with 0.015% butylhydroxytoluene and 0.018% dl-α-tocopheryl acetate to limit lipid peroxidation. Mice were kept on the diets for 12 wk. During the trial, body mass was measured weekly, and food was exchanged twice/wk to limit lipid peroxidation. To control the stability of dietary fatty acids, fats from diets were extracted, and fatty acids were derivatized with trimethylsulphonium hydroxide and analyzed by gas chromatography (Technische Universität München; ZIEL-Bioanalytics Unit, Freising, Germany). Fatty acid compositions (data not

Table 1. Composition of diets

Nutrient	C	HF	HF/n-3
Lipids, %			
Soybean oil	5.00	5.00	5.00
Palm oil		20.00	11.25
EPAX 1050 TG (DHA/EPA)			8.75
Cholesterol	0.013	0.038	0.021
Carbohydrates, %			
Corn starch	47.79	27.79	27.79
Maltodextrin	5.60	5.60	5.60
Sucrose	5.00	5.00	5.00
Cellulose	5.00	5.00	5.00
Protein, %			
Caseine	24.00	24.00	24.00
Antioxidants, %			
Butylhydroxytoluene	0.015	0.015	0.015
Dl-α-tocopheryl acetate	0.018	0.018	0.018
Others, %			
L-Cystine	0.20	0.20	0.20
Vitamins	1.20	1.20	1.20
Minerals and trace elements	6.00	6.00	6.00
Choline-chloride	0.20	0.20	0.20
Metabolizable energy, MJ/kg	15.50	19.80	19.80
Fat, %	13.00	48.00	48.00
Carbohydrates, %	64.00	34.00	34.00
Protein, %	23.00	18.00	18.00

C, control diet; HF, high-fat diet; HF/n-3, high-fat diet enriched with long-chain (LC-) n-3 polyunsaturated fatty acids (PUFA), eicosapentaenoic acid (EPA), and docosahexaenoic acid (DHA). Shown are %macronutrients and other ingredients in different diets. Nutrient composition was kept constant across different diets, except for corn starch and fat components. Metabolizable energy was calculated according to Atwater in MJ/kg (provided by Ssniff Spezialdiäten).

shown) of the experimental diets resulted in n-6/n-3 PUFA ratios of 9.85 (C), 13.5 (HF), and 0.84 (HF/n-3). Fatty acid patterns did not vary significantly after 2 mo of storage and were not affected by the sterilization method (data not shown). Body composition (i.e., fat mass and lean mass) was measured every other week by NMR spectroscopy. Food intake and feces production were measured over the period of 1 wk every other week. Animals were euthanized by cervical dislocation after the 12-wk feeding trial. All procedures applied throughout this study were conducted according to the German guidelines for animal care and approved by the government of Oberbayern, Germany.

NMR spectroscopy. Body composition was measured every other week to monitor changes in fat and lean mass using the whole animal body composition NMR analyzer The Minispec mq 7.5 (Bruker BioSpin, Rheinstetten, Germany). Time domain NMR analysis provides an accurate method for the measurement of adipose and lean tissue in live mice without a need for anesthesia. Individual animals were placed into a plastic restrainer inserted into the analyzer for ≤ 3 min. Before data acquisition, the NMR analyzer was calibrated with dissected adipose tissue and lean muscle.

Bomb calorimetry. Gross energy of fecal samples was determined with a Parr Instrument (Moline, IL) 6300 Calorimeter. For measurement, samples were homogenized with a TissueLyser II (Qiagen/Retsch, Hilden, Germany) and powder and then pressed as pills of \sim 1 g. The weighed pill was placed into the calorimeter and connected to an ignition thread, and energy (MJ/kg) per pill mass was determined by the software.

Sample collection, total RNA, and protein extraction. After the mice were euthanized in the postprandial state, body length (snout to base of the tail) was measured, and organs and tissues were immediately removed, weighed on a precision balance, snap-frozen, and stored at -80°C. For analysis, adipose tissue depots (mesenteric, epididymal, inguinal, and interscapular brown adipose tissue), liver, mucosa of the small intestine, and spleen were sampled. Obviously enlarged MLN were not observed, and therefore, MLN were not dissected out from MAT. Blood was collected from the vena cava inferior and plasma stored in either heparinized or EDTA-coated tubes (Sarstedt, Nuembrecht, Germany). To obtain homogenous tissue samples, tissues were ground in a frozen state with liquid nitrogen to tissue powder. Tissue powder aliquots were homogenized in Qiazol lysis reagent (Qiagen, Hilden, Germany) or radioimmunoprecipitation assay (RIPA) buffer (0.05 M Tris·HCl, 0.15 M NaCl, 1 mM EDTA, 0.2% SDS, 1% NP-40, and 0.25% Na-deoxycholate) for RNA or protein extraction, respectively. Total RNA was then extracted with chloroform and purified with the mRNeasy mini kit (Qiagen, Hilden, Germany) according to the manufacturer's instructions. DNA contamination was removed by on-column DNase I digestion (Qiagen). The concentration of the eluate was determined with a NanoDrop ND-1000 UV-Vis spectrophotometer (Peqlab, Erlangen, Germany) and the quality confirmed with the Agilent 2100 Bioanalyzer Nano kit (Agilent Technologies, Böblingen, Germany) according to the manufacturer's instructions and expressed as RNA integrity number.

For protein extractions, homogenates were kept in cold RIPA buffer with proteinase and phosphatase inhibitors (Sigma-Aldrich, Taufkirchen and Roche, Mannheim, Germany) and briefly centrifuged to remove cell debris. Protein concentration of extracts was then determined by bicinchoninic acid method (Pierce Thermo Scientific, Bonn, Germany) in a 96-well plate with a BSA standard at 562 nm in a UV-Vis spectrophotometer (Tecan, Groeding, Austria). Extracts were then diluted with 5× SDS-PAGE sample buffer (310 mM Tris·HCl, 5% SDS, 25% glycerol, 50 mM DTT, 2.5 mM EDTA, bromophenol blue) and stored at -20° C until use for SDS-PAGE and Western blotting.

Gene expression analysis. Expression of specific target genes was evaluated with reverse transcription-quantitative PCR (RT-qPCR). For each sample, 10 ng of extracted RNA was used per reaction using the QuantiTect quantitative, real-time one-step RT-PCR kit (Qiagen),

following the supplier's protocol. For primer design, nucleic acid sequences for genes and transcript variants were retrieved from ENSEMBL and NCBI nucleotide databases and compared with the Mouse Genome Informatics database. Primer sequences were retrieved using NCBI Sequence Viewer and NCBI Primer Blast and modified using OligoCalc and IDT Oligo Analyzer to search for in silico primer characteristics. Sequence specificity was checked with Basic Local Assignment Alignment Search Tool (http://www.ncbi. nlm.nih.gov/tools/primer-blast/) analysis, University of California Santa Cruz in silico PCR (http://genome.ucsc.edu/), and conventional PCR to determine optimal annealing temperatures (Table 2). For Spp1 gene expression analysis, a commercially available primer assay was used additionally (Qiagen). RT-qPCR was performed using SYBR Green I dye and a Mastercycler ep realplex⁴ S (Eppendorf, Hamburg, Germany). The following thermal cycling conditions were used: 50°C (cDNA synthesis) for 30 min and 95°C for 15 min (RT enzyme inactivation), followed by 40 cycles at 95°C for 15 s, 60°C for 30 s, and 72°C for 30 s. The PCR was concluded with a melting curve analysis of the PCR product (1.75°C/min). C_q values were retrieved from the realplex 2.0 software (Eppendorf) and analyzed according to the $\Delta\Delta C_q$ method (35). To normalize the data the following genes were used as invariant controls: β-actin (Actb), glyceraldehyde-3-phosphate dehydrogenase (Gapdh), hypoxanthine-guanine phosphoribosyltransferase 1 (Hprt1), cyclophilin B (CypB), and heat shock protein 90α (cytosolic) and class B member 1 (Hsp90αb1). For all groups, data were expressed as means ± SE relative to control samples.

For each RT-qPCR, 10 ng of total RNA was applied. As RT-qPCR assay controls, nontemplate assays and (-)-RT assays were included for every primer used. Target specificity was examined by melting curve analysis and agarose gel electrophoresis. Additionally, primer PCR efficiency was determined with LinRegPCR version 12.16 (J. M. Ruijter, Academic Medical Center) using the raw fluorescence data from RT-qPCR.

The relative uncoupling protein 1 (UCP1) gene expression capacity index was calculated as follows:

$$\frac{\text{relative UCP expression} \times \text{total iBAT tissue (mg)}}{\text{body mass (mg)}} \times 100\%.$$

RT-qPCR arrays. Pathway-specific RT² Profiler RT-qPCR arrays for "T and B cell activation" (cat. no. PAMM-053; SABiosciences/Qiagen) and "endothelial cell biology" (cat. no. PAMM-015; SABiosciences/ Qiagen, Hilden, Germany) were used with specific primers for 84 target genes, housekeeping genes, and controls supplied in a 96-well plate. RT-qPCR was performed according to the supplier's instructions. For each dietary group, a separate plate was used. Equal amounts of RNA from four animals per dietary group were pooled, and 1 µg of pooled RNA was reverse transcribed according to the manufacturer's instructions. Along with a RT-qPCR master mix containing SYBR Green I, the newly synthesized cDNA was added to the 96-well plate, and the RT-qPCR was performed according to instructions. For analysis baseline was set automatically, but threshold was set to 400 units of fluorescence for all analyses. C_q values were normalized with the given housekeepers (Actb, Hprt1, Gapdh, and Hsp 90α b) and fold changes (FC) calculated with a web-based analysis tool provided by the manufacturer (http://pcrdataanalysis.sabiosciences.com/) according to the $\Delta\Delta C_q$ method.

Blood parameters and glucose tolerance test. To assess fasting blood parameters during the feeding trial, mice were fasted for 5 h, and blood was withdrawn by tail vein bleeds and collected in EDTA-coated tubes (Sarstedt, Nuembrecht, Germany). For the assessment of glucose tolerance after 12 wk of feeding, mice fasted for 6 h were injected with a sterile glucose solution (2 g/kg body mass; B. Braun, Melsungen, Germany) intraperitoneally. Blood was withdrawn before and at 15, 30, 60, and 120 min postinjection, and blood glucose levels

Table 2. Primer sequences

Target Gene	Primer						
Acacα							
(Qiagen				ОТО	15544	41	
order no.) Acox1				Q10	13344	41	
Forward	5'-GAG	ATG	GAT	ААТ	GGC	TAC	CTG AAG-3'
Reverse							TCA GC-3'
Actb							
Forward	5'-CCA						CC-3'
Reverse	5'-GCC	ACA	GGA	TTC	CAT	ACC	CAA GA-3'
CD4 Forward	5'-TAG	٨٥٥	٨٥٥	mm.c	CCC	TITIC	CC 2'
Reverse							CCA GC-3'
CD8α	3 001	001	011	100	101	101	0011 00 5
Forward	5'-AGA	AAG	TGA	ACT	CTG	CTG	CTA CCA A-3
Reverse	5'-AAT	CTT	CTG	GTC	TCT	GGG	GCT G-3'
СурВ							
Forward							GAA-3'
Reverse	5'-TCC	TTG	ATG	ACA	CGA	TGG	AA-3
Cpt1a Forward	5'-GTC	CCA	CCT	GTC	ΔΔΔ	САТ	ACC G-3'
Reverse							TTA ACC-3'
Emr1 (F4/80)							
(Qiagen							
order no.)		QT00099617					
Fads1	<i>51</i> + 22	~ . ~	~	~			g.g.m. + + 2/
Forward	5'-ACC 5'-CAG						GCT AA-3'
Reverse Fads2	3 -CAG	CCA	CAI	CCA	GUA	GUA	G-3
Forward	5'-ACC	GTG	GCA	AAA	GCT	СТС	AG-3'
Reverse							AGG C-3'
Foxp3 (Qiagen							
order no.)	QT00138369						
Gapdh	£L aam	001	G A A	100	таа	G 4 4	am , ma 2/
Forward Reverse							GTA TG-3' AAG TC-3'
Hprt1	J -GAG	166	GAG	110	CIG	110	AAG 10-3
Forward	5'-GTC	GTG	ATT	AGC	GAT	GAT	GAA CC-3'
Reverse	5'-GTC	TTT	CAG	TCC	TGT	CCA	TAA TCA G-3
Hsp90αb1							
Forward	5'-AGG						
Reverse	5'-TTT	TTC	TTG	TCT	TTG	CCG	CT-3'
Icam1 Forward	5' CTC	πлс	۸۸۵	ффф	тст	ССТ	CCG GT-3'
Reverse							CGA C-3'
I1-10	5 001	0110	11110	11110	0110	011	0011 0 5
Forward	5'-GCT	GTC	ATC	GAT	TTC	TCC	CCT G-3'
Reverse	5'-AGA	CAC	CTT	GGT	CTT	GGA	GCT T-3'
Itgax	~!·						2/
Forward							AGA C-3'
Reverse Lep	3 -CTG	AAG	CTG	GCT	CAT	CAC	AGC-3'
Forward	5'-ACA	ттт	CAC	ACA	CGC	AGT	CGG-3'
Reverse	5'-AGG						
Mcp-1							
Forward							AAC G-3'
Reverse	5'-GCT	TGG	TGA	CAA	AGA	CTA	CAG CTT-3'
Mrc1	51 000	100	4.00		000	000	A ED 21
Forward Reverse	5'-GCC						AT-3' GGT G-3'
Spp1	J-GGA	GII	GII	GIG	GGC	TOT	GG1 G-3
Forward	5'-CCA	GAT	ССТ	АТА	GCC	ACA	TGG CT-3'
Reverse	5'-AGC						
Qiagen							
order no.	QT00157724						
Scd-1	~!	m « =	a	. ~ .	a	a = -	a 21
Forward	5'-GGC						
Reverse	5'-AAG	TOI	CGC	CCC	AGC	AGT	H-3

Continued

Table 2.—Continued

Target Gene	Primer							
Tek								
Forward	5'-GAT	GTG	ACC	AGA	GAA	TGG	GCG	AA-3'
Reverse	5'-AGG	AAG	GAT	GCT	TGT	TGA	CGC	AT-3'
Tnfα								
Forward	5'-CCA	CGT	CGT	AGC	AAA	CCA	CCA	A-3'
Reverse	5'-GAA	GAG	AAC	CTG	GGA	GTA	GAC	AAG G-3'
Ucp1								
Forward	5'-CTG	GGA	GAG	AAA	CAC	CTG	CCT	C-3'
Reverse	5'-CTC	TGT	AGG	CTG	CCC	AAT	GAA	CA-3'
Vcam1								
Forward	5'-CGT	GGA	CAT	CTA	CTC	TTT	CCC	CA-3'
Reverse	5'-TGT	CTG	GAG	CCA	AAC	ACT	TGA	CC-3'

Acacα, acetyl-coenzyme A carboxylase- α ; Acox1, acyl-coenzyme A oxidase 1; Actb, β-actin; CypB, cyclophilin B; Cpt1a, carnitine palmitoyl transferase 1a; Emr1, EGF-like module containing, mucin-like, hormone receptor-like sequence 1; Fads1 and -2, fatty acid desaturase 1 and 2; Foxp3, forkhead box protein P3; Hprt1, hypoxanthine-guanine phosphoribosyltransferase 1; Hsp90 α b, heat shock protein 90 α (cytosolic) and class B member 1; Icam1, intercellular adhesion molecule 1; Itgax, integrin α X; Lep, leptin; Mcp-1, monocyte chemoattractant protein-1; Mrc1, mannose receptor C type 1; Spp1, secreted phosphoprotein 1; Scd-1, stearoyl-coenzyme A desaturase; Tek, TEK tyrosine kinase, endothelial; Ucp1, uncoupling protein 1; Vcam1, vascular cell adhesion molecule 1.

were measured directly using a hand-held device (FreeStyle Lite; Abbott Laboratories, Abbott Park, IL).

Chemical analysis. To determine hepatic triacylglycerol (TAG) content, liver tissues were ground in a frozen state with liquid nitrogen and dissolved in 0.9% NaCl. TAG were extracted as follows; homogenates were incubated with 0.5 M ethanolic KOH (30 min, 71°C), 0.15 M magnesium sulfate was added, and after centrifugation at 13,000 g for 10 min, TAG concentrations were determined using a commercial enzymatic colorimetric kit, following the manufacturer's instructions (Triglycerides liquicolor^{mono}; Human, Wiesbaden, Germany), at 500 nm on a UV-Vis spectrophotometer (Amersham/GE Healthcare, Munich, Germany). Results were normalized to the protein content of the samples as determined by the Bradford assay. For measurement of NEFA in plasma, samples were processed and analyzed with the NEFA-HR(2) kit (Wako Chemicals, Neuss, Germany) according to the manufacturer's protocol.

Western blot. Equal amounts of protein (40 µg/lane protein) were resolved by a 12.5% SDS-PAGE. Subsequently, proteins were transferred to a nitrocellulose membrane using semidry blotting (Biometra, Göttingen, Germany). The membrane was washed with Tris-buffered saline (TBS) and blocked with 2% ECL Advance blocking reagent (GE Healthcare, Munich, Germany). After washing with TBS + 0.1%Tween-20 (TBS-T; Sigma-Aldrich, Taufkirchen, Germany), membranes were incubated with primary antibody [monoclonal mouse antimouse osteopontin (OPN) (SC-21742, Santa Cruz Biotechnology, Heidelberg, Germany), 1:500 in TBS-T + 2% ECL Advance blocking reagent] at 4°C overnight. Detection using an IRDye680CW-conjugated goat anti-rabbit secondary antibody was performed with the Odyssey Infrared Detection system (LI-COR Biotechnology, Hamburg, Germany). As an invariant control, β-actin protein expression was used (polyclonal rabbit anti-human β-actin no. 4967, Cell Signaling Technology, Frankfurt, Germany). Densitometric analysis was performed using Odyssey application software version 3.0 (LI-COR Biotechnology).

Histological analysis. To detect hepatic lipid accumulation by Oil Red O staining, fresh liver tissue was embedded in OCT TissueTek freezing medium (Sakura Finetek, Staufen, Germany) and cut in 10-μm sections with a Cryo-Star HM 560 MV (Microm/Thermo Fisher, Walldorf, Germany). Sections were fixed briefly in 10% formalin and washed with water and isopropanol, followed by staining and counterstaining performed with freshly prepared Oil Red O solution and hematoxylin (Roth, Karlsruhe, Germany), respectively. After mounting in aqueous

medium (Merck, Darmstadt, Germany), sections were photographed with a DMI 4000 B microscope and Leica Application Suite version 3.7 (Leica Microsystems, Wetzlar, Germany).

For determination of adipocyte cross-sectional area, adipose tissue was fixed in 4% paraformaldehyde overnight, dehydrated, and embedded in paraffin. Sections were cut at 7 μm and stained with hematoxylin and eosin. Photographs were taken with a DMI 4000 B microscope and Leica Application Suite version 3.7 (Leica Microsystems) at $\times 200$ magnification, and the area was determined using the polygon and measurement tool in Image J (Open Source; National Institutes of Health, Bethesda, MD). For quantitative analysis, five representative areas per slide were chosen for analysis from three animals (9). Average cell area per animal was calculated with Microsoft Office Excel (Microsoft) and analyzed with Prism 5 (GraphPad).

For immunohistochemistry of paraformaldehyde-fixed paraffinembedded adipose tissues, 6-µm-thick sections from MAT and EAT were dewaxed and stained with specific primary antibodies, followed by antigen signal detection using corresponding specific secondary antibodies combined with the Bond Polymer Refine Detection kit (cat. no. DS9800; Leica Microsystems) and a polymeric horseradish peroxidase linker antibody conjugate with 3,3'-diaminobenzidine tetrahydrochloride. Finally, sections were counterstained with hematoxylin (Roth). Primary antibodies to macrophage antigens were monoclonal rat anti-F4/80 (T-2006; BMA Biomedicals, Augst, Switzerland), monoclonal hamster anti-mouse CD11c (cat. no. 553799; BD Biosciences, Heidelberg, Germany), and polyclonal rabbit anti-human CD206/ MRC1 (cat. no. 18704-1-AP; Proteintech, Chicago, IL). Digital images were taken with a DMI 4000 B microscope and Leica Application Suite version 3.7 (Leica Microsystems, Wetzlar, Germany) at ×200 magnification. CLS were defined as at least three positively stained cells surrounding an adipocyte. CLS density was defined as number of CLS per total section area. A minimum of four sections per tissue of each animal (n = 8/group) were analyzed.

For T cell differentiation marker expression analysis, 6- μ m cryosections from spleen tissues embedded in OCT TissueTek freezing medium (Sakura Finetek, Staufen, Germany) were fixed briefly in acetone and processed for staining with the following primary antibodies and antigen signal detection system. Primary antibodies were monoclonal rat anti-CD4 mouse (cat. no. 550278; BD Biosciences) and monoclonal rat anti-mouse CD8 α (cat. no. 553027; BD Biosciences). Primary antibodies were detected by antigen signal detection,

using corresponding specific secondary antibodies combined with the Bond Polymer Refine Detection kit (cat. no. DS9390; Leica Microsystems), with Fast Red as substrate chromogen and hematoxylin (Roth) counterstaining. Digital images were taken with a DMI 4000 B microscope and Leica Application Suite version 3.7 (Leica Microsystems) at $\times 100$ magnification. Antigen signal-positive stained areas were quantified using Image-Pro Plus version 7.0 software (Media Cybernetics), analyzed with Excel 2010 (Microsoft) and Prism 5 (GraphPad), and expressed as a percentage of total section area. Four tissue sections per spleen of each animal (n = 4-6/group) were analyzed.

ELISA. Fasting plasma insulin was determined using EDTA-stabilized plasma and the Ultra Sensitive Mouse Insulin ELISA Kit (Crystal Chem). Plasma OPN levels were determined using heparinstabilized plasma and the Quanitkine Mouse Osteopontin Immunoassay kit (cat. no. MOST00; R & D Systems, Wiesbaden, Germany). Plasma serum amyloid A (SAA) levels were determined using the mouse SAA ELISA kit (cat. no. E-90SAA; ICL). Monocyte chemoattractant protein-1 (MCP-1) levels were determined using heparinstabilized plasma and the mouse MCP-1 ELISA Ready-SET-Go! set (cat. no. 88-7391; eBiosciences, Frankfurt, Germany).

Statistical analysis. All data were expressed as means \pm SE. Statistical analyses were performed using Prism 5 (GraphPad, La Jolla, CA). Differences were considered statistically significant with P < 0.05, P < 0.01, and P < 0.001 compared with control group or HF high-fat group. One-way ANOVA was used to detect differences between dietary groups with Tukey's posttest to identify significant differences. For body mass curves and glucose tolerance tests, two-way ANOVA with Bonferroni posttest was used to identify statistically significant differences between dietary groups. Correlation analysis between gene expression and mass was performed using the Pearson test.

RESULTS

LC-n-3 PUFA-enriched high-fat diet limits obesity development by reducing adipose tissue mass. Data on body mass development showed that the initial body mass of mice was similar among the three dietary groups, but as early as 3 wk on the diet, body mass of HF mice was significantly higher than controls (Table 3 and data not shown). Compared with controls, the body mass of the HF/n-3 group did not reach statistically different

Table 3. Effects of LC-n-3 PUFA on body and organ mass, food intake, and energy intake and excretion

	C	HF	HF/n-3
Body mass, g			
Initial	21.7 ± 0.4	22.1 ± 0.4	21.7 ± 0.3
Week 3	24.6 ± 0.5	28.1 ± 0.6^{a}	26.5 ± 0.5
Week 7	27.3 ± 0.6	33.1 ± 1.0^{a}	31.1 ± 0.8^{a}
Final	31.4 ± 1.1	40.8 ± 1.3^{a}	$36.8 \pm 0.8^{a,b}$
Change	9.7 ± 0.8	18.7 ± 1.2^{a}	$15.1 \pm 0.8^{a,b}$
Total white adipose tissue, mg	$1,887.8 \pm 271.0$	$5,129.8 \pm 357.4^{a}$	$4,051.6 \pm 304.1^{a,b}$
IAT	316.8 ± 47.2	898.0 ± 51.8^{a}	$710.8 \pm 52.3^{a,b}$
MAT	277.2 ± 34.7	662.9 ± 62.7^{a}	$510.0 \pm 49.2^{a,b}$
EAT	965.3 ± 128.1	$2,567.3 \pm 198.5^{a}$	$1,977.1 \pm 141.5^{a,b}$
PRAT	328.6 ± 64.7	$1,001.7 \pm 80.9^{a}$	853.7 ± 72.2^{a}
BAT, mg	179.3 ± 21.2	312.0 ± 15.5^{a}	$246.8 \pm 18.2^{a,b}$
Liver, mg	$1,401.4 \pm 55.3$	$1,609.3 \pm 66.6^{a}$	$1,493.2 \pm 37.6$
Spleen, mg	88.2 ± 4.5	87.4 ± 4.9	$125.0 \pm 7.8^{a,b}$
Intake and excretion			
Food intake, g/wk	22.0 ± 0.4	20.9 ± 0.3	22.23 ± 0.4
Energy intake, kJ/wk	341.2 ± 6.6	413.6 ± 6.1^{a}	$439.70 \pm 7.6^{a,b}$
Energy excretion, kJ/wk	30.4 ± 0.6	33.1 ± 1.3	29.02 ± 0.7^{b}

Values were calculated as means \pm SE (body and organ mass, n=9-12; food intake, n=7; energy intake and excretion, n=4-5) per dietary group for 12-wk feeding. IAT, inguinal subcutaneous adipose tissue; MAT, mesenteric adipose tissue; EAT, epididymal adipose tissue; PRAT, perirenal adipose tissue. Superscripted letters a and b indicate a significant difference (P < 0.05) at each time point compared with C or HF group, respectively. Statistical analysis was performed by 1-way ANOVA and Tukey's posttest.

levels until 7 wk of feeding. After the 12-wk feeding period, HF and HF/n-3 led to a significant body mass increase compared with C diet, whereas body length was similar between dietary groups (C, 9.17 ± 0.17 cm; HF, 9.46 ± 0.13 cm; HF/n-3, 9.30 ± 0.08 cm). Body mass development was mirrored by increased fat mass, as determined by NMR spectroscopy (Fig. 1A). Fat mass in HF and HF/n-3 mice reached significantly higher levels after 5 and 8 wk, respectively, than in controls. Although the lean mass in the HF and HF/n-3 group was higher in week 3, this effect was lost afterward, and lean mass increased only slightly in all three groups (Fig. 1B). During the feeding trial, the weekly food intake was not statistically different between the dietary groups (Table 3). Energy intake, calculated by multiplying weekly food intake with metabolizable energy (Table 1), showed that mice of both the HF and HF/n-3 groups ingested more energy per week than controls (Table 3). Interestingly, HF/n-3 animals ingested slightly more energy than HF animals but excreted less energy, as determined by bomb calorimetry of fecal samples (Table 3). Notably, overall energy assimilation was higher for HF/n-3 than HF, although HF/n-3 mice weighed less than HF mice. At the end of the feeding period, adipose tissue analysis revealed that all fat depots of mice on high-fat diets were substantially heavier than in controls (Table 3). For HF/n-3 mice, however, MAT, EAT, inguinal subcutaneous fat, and interscapular brown adipose tissue (iBAT) exhibited significantly lower masses compared with HF mice. This effect was not significant in perirenal/retroperitoneal adipose tissues but indicated the same trend. Interestingly, liver mass was only significantly higher in HF mice than in controls. Surprisingly, spleen mass was significantly increased 1.4-fold in HF/n-3 mice compared with controls, but not in HF mice (Table 3).

LC-n-3 PUFA have no differential effect on mass and leptin gene expression of VAT depots but differentially affect their morphology. MAT and EAT mass were increased significantly on both high-fat diets, whereas, compared with HF, HF/n-3

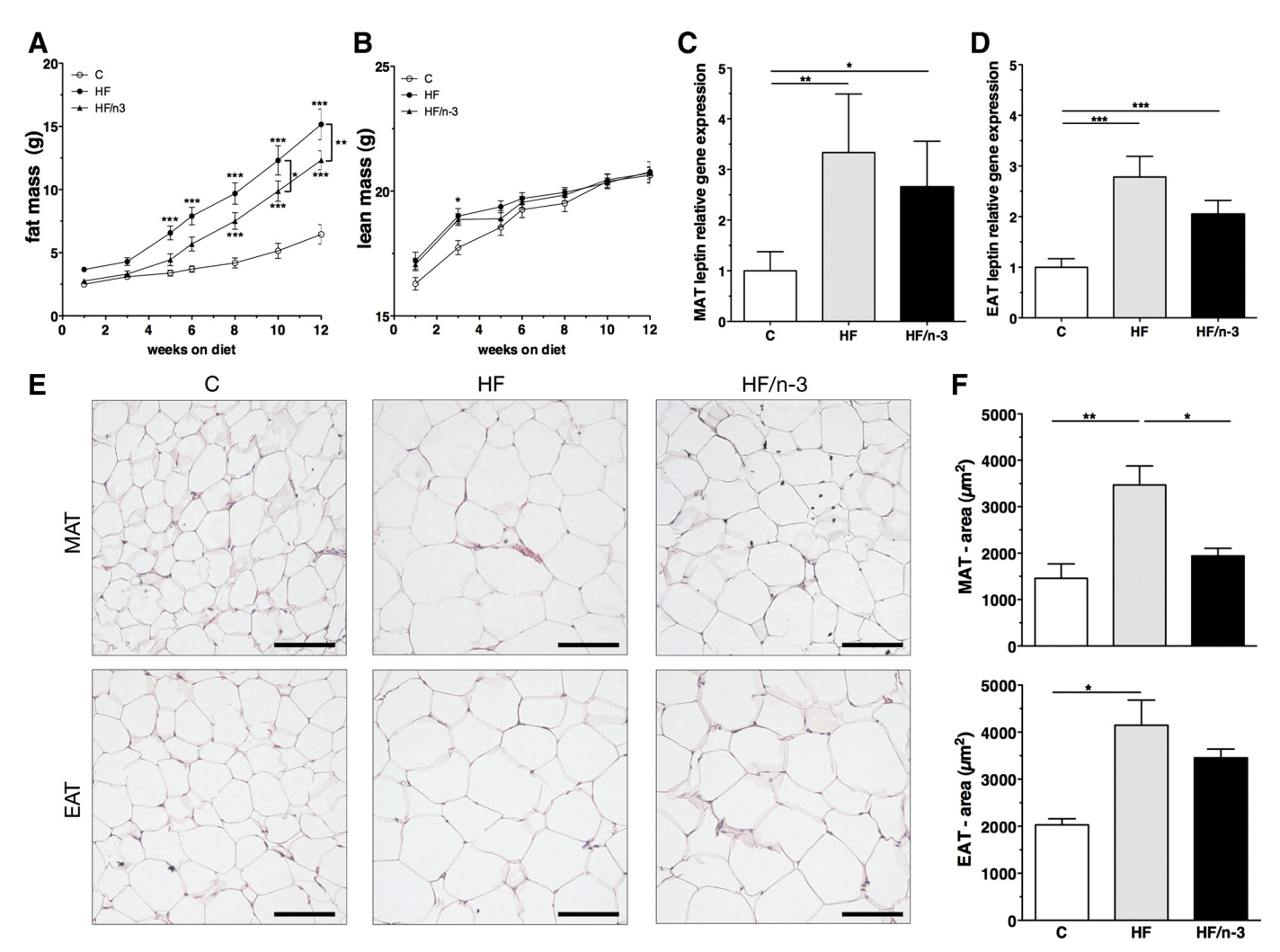


Fig. 1. Characterization of body composition, leptin gene expression, and adipocyte cross-sectional area in mesenteric (MAT) and epididymal adipose tissue (EAT). Male C57BL/6J mice (n=9-12) fed either control (C), high-fat diet (HF), or long-chain (LC)-n-3 polyunsaturated fatty acid (PUFA)-enriched high-fat diet (HF/n-3) for 12 wk show increased body mass (data not shown). Fat (A) and lean mass (B) determined every other week by NMR spectroscopy are shown. Shown are mean leptin mRNA gene expression levels in MAT (C) and EAT (D) relative to controls after 12 wk of feeding measured by RT-quantitative (q)PCR (n=8-12). Data were analyzed by $\Delta\Delta C_q$ method and normalized to B-actin, Gapdh, and hypoxanthine-guanine phosphoribosyltransferase 1 (Hprt1) gene expression. E: representative hematoxylin and esoin-stained paraffin sections of MAT and EAT from C, HF, or HF/n-3 after 12 wk of feeding (n=3). Scale bar indicates 100 μm. E: graphs show mean cross-sectional area/cell in μm² of stained paraffin sections from MAT and EAT. All data are means E SE. Statistical analysis was performed using 2-way ANOVA and Bonferroni posttest for body composition and 1-way ANOVA and Tukey posttest for gene expression and histological analyses. *P < 0.05, *E0, *E1, and *E2 = 0.01, and *E3 = 0.001, significant differences compared with control or between groups as indicated.

mice showed a significantly lower adipose tissue mass (Table 3). Leptin (Lep) mRNA levels were significantly elevated in adipose tissues from HF and HF/n-3 mice compared with controls, and a trend for lower levels in HF/n-3 mice than in HF mice was observed (Fig. 1, C and D). Interestingly, the gene expression was highly correlated with body mass and more pronounced in MAT than in EAT (MAT: $r^2 = 0.7376$; EAT: $r^2 = 0.5723$; P < 0.0001). Analysis of adipocyte cross-sectional areas in histological tissue sections from MAT and EAT revealed that adipocytes from HF mice were significantly larger than in controls. In contrast, increased MAT mass in HF/n-3 mice exhibited no significant enlargement in adipocyte size (Fig. 1, E and E). Adipocyte cross-sectional area in MAT was significantly decreased by 43% compared with HF, whereas this effect was diminished in EAT (-19%).

LC-n-3 PUFA-enriched high-fat diet improves plasma insulin levels and lipid parameters. After 12 wk of feeding, fasting plasma insulin levels were significantly elevated 1.9-fold upon HF compared with C diet, whereas insulin levels of HF/n-3 and C diet were similar (Fig. 2A). Furthermore, adverse effects of high-fat diets on glucose tolerance were observed. Comparing HF and HF/n-3 with C diet, basal glucose levels of animals on high-fat diets already differed, and an intraperitoneal glucose tolerance test showed a delayed glucose clearance (Fig. 2B). Blood glucose values peaked after 30 min in C and HF/n-3 mice but not before 60 min in HF mice. After 120 min, HF animals still showed statistically significant elevated glucose levels, whereas a strong trend for improved glucose clearance was observed upon HF/n-3 compared with HF (C, 195 ± 14.8 mg/dl; HF, 313 ± 36.6 mg/dl; HF/n-3, 265 ± 14.1 mg/dl; ANOVA, P = 0.0043, but only C vs. HF, P < 0.01). Area under the curve analysis, determined for the 30- to 120-min time interval, showed the same trend [C: $10,565 \pm 2,461$ arbitrary units (AU); HF: $16,400 \pm 2,534$ AU; HF/n-3: $14,056 \pm 1,542$ AU; P = 0.1986]. To find out whether the HF/n-3 exerts lipid-lowering effects, the ectopic deposition and content of TAG in mice were assessed by light microscopy of Oil Red O-stained liver sections (Fig. 2, C-E) and by biochemical analysis (Fig. 2F), respectively. Substantial accumulations of lipid droplets were found only in hepatocytes of HF mice (Fig. 2D). Moreover, hepatic TAG concentrations were significantly higher for HF animals than controls, whereas hepatic TAG levels upon HF/n-3 were not significantly different from those in controls (Fig. 2F). Additionally, we observed a significant decrease in nonfasting plasma nonesterified fatty acid (NEFA) only in HF/n-3 mice (Fig. 2G). For HF/n-3 mice, improved hepatic TAG and plasma NEFA levels and lower body mass, despite higher energy assimilation than in HF animals, indicated a LC-n-3 PUFA-induced increase in energy expenditure. To further characterize this effect, the gene expression of key regulators and enzymes involved in hepatic lipogenesis, β-oxidation, and endogenous LC-PUFA synthesis, as well as in iBAT energy expenditure, was examined by RT-qPCR (Fig. 2H). A significantly strong reduction of hepatic mRNA expression for the lipogenesis-related enzymes stearoyl-coenzyme A desaturase (Scd-1) and acetyl-coenzyme A carboxylase-α (Acacα) was detected for HF/n-3 mice compared with HF and control mice. Hepatic mRNA levels for the peroxisomal fatty acid oxidation marker acyl-coenzyme A oxidase 1 (Acox1) were significantly upregulated in both HF and HF/n-3 mice, whereas carnitine palmitoyltransferase 1a (Cpt1a) mRNA was

only significantly upregulated by HF compared with C and HF/n-3. mRNA levels for fatty acid desaturases 1 (Fads1; Fig. 2H) and 2 (Fads2), which are the key enzymes of endogenous LC-PUFA synthesis, were only significantly downregulated by HF/n-3 (Fads2 mRNA expression: C, 1.00 ± 0.16 ; HF, 0.98 ± 0.13 ; HF/n-3, 0.23 ± 0.04 ; P < 0.0001). Interestingly, UCP1 mRNA levels were significantly upregulated ~ 1.5 -fold in iBAT upon HF/n-3 compared with the HF and C diet. Considering the differences of iBAT mass and body mass between the three dietary groups in week 12 (Table 3), the determined relative Ucp1 gene expression capacity index was still 1.7- and 1.2- fold higher for HF/n-3 mice compared with C and HF mice, respectively, and 1.3-fold higher for HF than controls (C, $0.67 \pm 0.07\%$; HF, $0.86 \pm 0.05\%$; HF/n-3, $1.11 \pm 0.1\%$; P < 0.0045).

HF/n-3 upregulates mRNA expression of genes involved in immune cell activation in MAT. To study the impact of LC-n-3 PUFA on the expression of pro- and anti-inflammatory genes in VAT, first, the mRNA levels of 84 genes involved in macrophage and T cell and B cell activation were measured by gene expression array experiments for MAT of each dietary group in an explorative approach. Compared with HF, MAT from HF/n-3 mice surprisingly revealed an expression profile of predominantly upregulated genes. Fifty-one percent of the analyzed genes displayed an increased expression with a FC of >1.2 (Fig. 3A, *left*; for a detailed list, see Table 4), whereas almost the same number of genes (44%) was not affected at all by LC-n-3 PUFA treatment ("no change"), and only 5% of the genes were downregulated (FC < -1.2). The very few downregulated genes upon HF/n-3 were Nos2 and Cdkn1a. Next, the genes, identified by HF/n-3-induced elevation (FC > 1.2) of expression, were arranged according to their function in activation, proliferation, or differentiation processes of T cells and B cells to the following groups: T cell immunity, B cell immunity, and T and B cell immunity (Fig. 3A, right). Fifty percent of the genes belonged to the T cell immunity group, 28% to the B cell immunity group, and 12% to the T and B cell immunity group. In addition, genes with highly upregulated mRNA levels in MAT upon both high-fat diets compared with controls were identified, for example, Jagged2 and E3 ubiquitin protein ligase Wwp1, which are involved in T cell differentiation (71, 82). Interleukin-7, which is involved predominantly in B cell proliferation (44), was upregulated 2.22- and 1.56fold in HF/n-3 and HF animals over controls, respectively. Interestingly, genes that were downregulated upon HF and highly upregulated upon HF/n-3 were the genes for the proinflammatory secreted phosphoprotein 1 (0.62- vs. 9.45-fold) and the T_h1-cell type differentiation promoting cytokine interferon-y.

For validation of highly regulated genes related to obesity and inflammation, we focused on the gene for secreted phosphoprotein 1 (SPP1), also known as OPN. OPN is recognized as a T cell-derived chemoattractant for macrophages (76), and it is expressed in adipocytes (31). Furthermore, OPN can be found at high levels in blood plasma of mice fed high-fat diets, and it is functionally implicated in obesity (19, 48). mRNA expression analysis in biological replicates of VAT by RT-qPCR showed that SPP1 mRNA levels were strongly increased in MAT and even more so in EAT in HF/n-3 animals compared with controls (Fig. 3B). This finding was also confirmed by using an independent set of commercially available primers in MAT (data not shown). Western blot and densitometric analysis detected elevated OPN levels in MAT from HF/n-3 and HF mice, but the significant

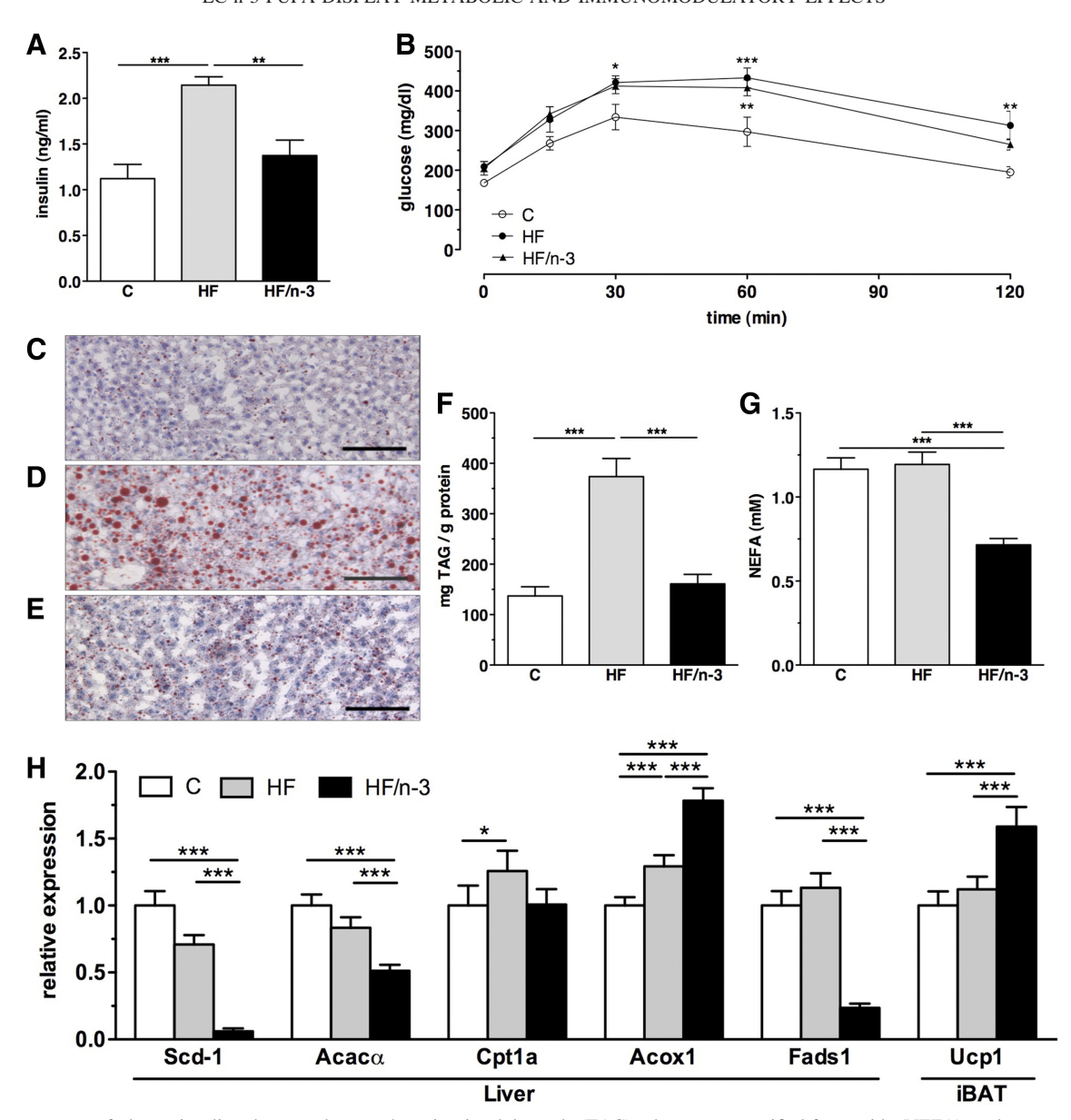


Fig. 2. Measurements of plasma insulin, glucose tolerance, hepatic triacylglycerols (TAG), plasma nonesterified fatty acids (NEFA), and gene expression. All data are means \pm SE and were collected from mice after 12 wk of feeding either C, HF, or HF/n-3. *A*: insulin in plasma of mice (n=9-12) was determined after 5 h of fasting. Blood glucose levels were measured by intraperitoneal glucose tolerance test before injection of glucose (0 min) and 15, 30, 60, and 120 min postinjection (*B*). Oil Red O and hematoxylin stained liver cryosections from C (*C*), HF (*D*), and HF/n-3 (*E*) mice. Scale bar indicates 100 μm. *F*: hepatic TAG were quantified and normalized to hepatic protein content (n=10-12). *G*: levels of nonfasting plasma NEFA are shown (n=10-12). *H*: gene expression data for stearoyl-coenzyme A desaturase (Scd-1), acetyl-coenzyme A carboxylase-α (Acacα), carnitine palmitoyl transferase 1a (Cpt1a), acyl-coenzyme A oxidase 1 (Acox1), and fatty acid desaturase 1 (Fads1) in liver and for uncoupling protein 1 (UCP1) in interscapular brown adipose tissue (iBAT) relative to C group by RT-qPCR (n=10-12) were retrieved after 12 wk of feeding. Data were analyzed by the ΔΔC_q method and normalized to β-actin, Gapdh, Hprt1, cyclophilin B (CypB), and heat shock protein 90α (cytosolic) and class B member 1 (Hsp90αb1) gene expression. Statistical analyses for insulin, TAG, NEFA quantification, and gene expression were performed using 1-way ANOVA and Tukey posttest and 2-way ANOVA and Bonferroni posttest for intraperitoneal glucose tolerance test analysis. *P < 0.05, **P < 0.01, and ***P < 0.001, significant differences compared with control or between groups as indicated.

differences as observed for mRNA levels were absent (Fig. 3, C and D). Measurements of plasma OPN levels by ELISA did not reveal different levels between the groups after 12 wk of feeding (Fig. 3E). Since our gene expression array experiments pointed to T and B cell activation upon HF/n-3, we examined whether T cell activation is associated with changes in CD4- and CD8 α -expressing T cell populations, which may vary depending on T cell activation-induced proliferation or apoptosis. Compared with controls, mRNA expression analysis for CD4 and CD8 α , as well as

for the regulatory T cell marker forkhead box protein P3 (Foxp3) (Fig. 3B) of MAT, showed that CD8 α mRNA was significantly reduced only in HF/n-3 mice, and a trend for diminished CD8 α levels was measured in HF mice. In addition, only trends for decreased CD4 and FoxP3 mRNA levels were detected in MAT from HF and HF/n-3 mice.

Differential gene expression of pro- and anti-inflammatory markers in MAT and EAT. To characterize the expression of inflammatory markers in MAT, EAT, and blood plasma, we

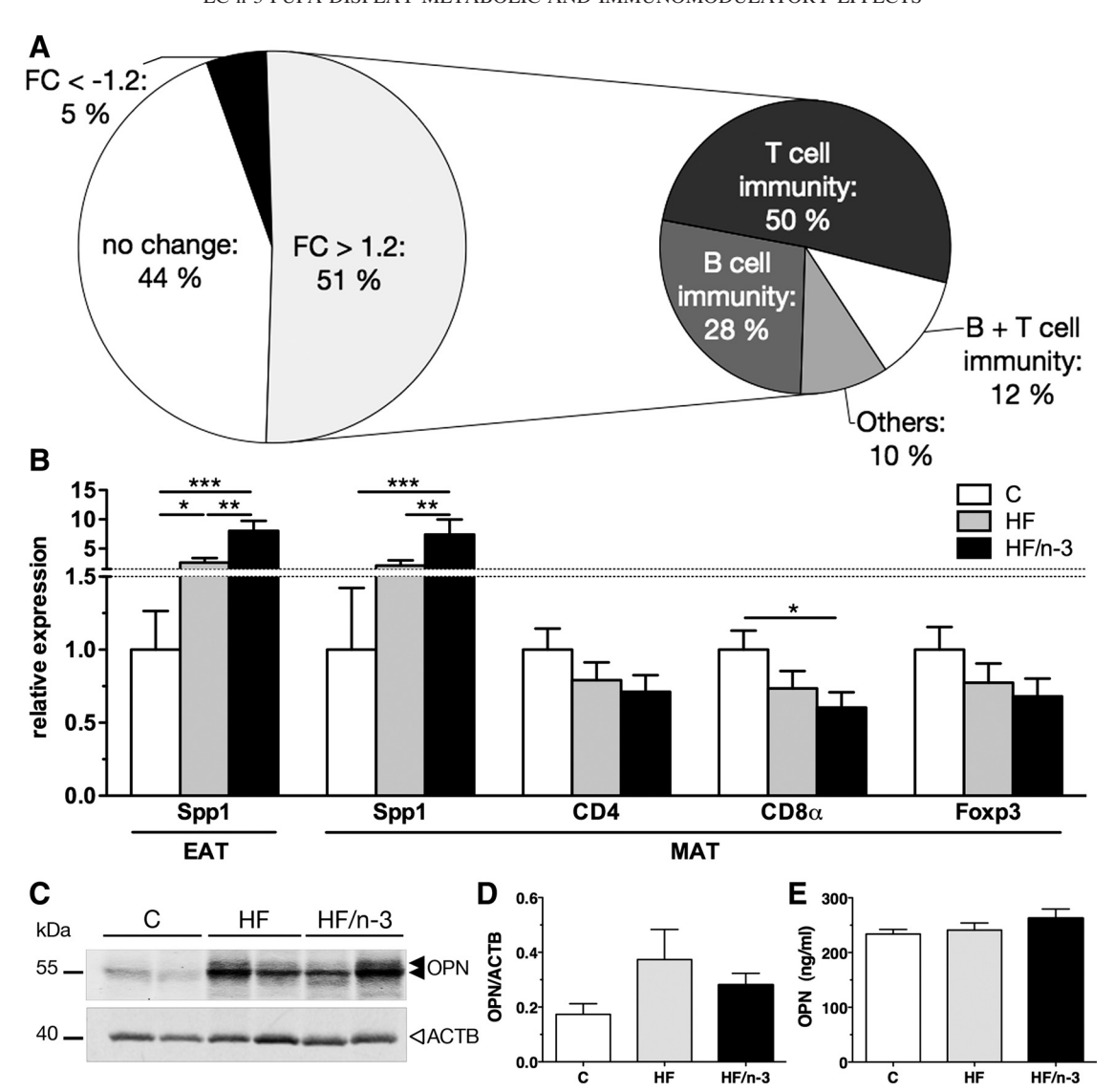


Fig. 3. Explorative gene expression array analysis of MAT, quantitative gene expression analyses in visceral adipose tissue (VAT), and osteopontin (OPN) protein expression in VAT and plasma. *A*: illustration of data from explorative gene expression analysis in MAT using RT² Profiler RT-qPCR array for 84 marker genes involved in macrophage and T and B cell activation. *Left*: graduation of analyzed genes in percentages displaying gene expression fold changes (FC) larger and smaller than 1.2 and without changes in HF/n-3 mice relative to HF mice. *Right*: genes with FC > 1.2 (shown at *left*) were arranged to the groups T cell immunity, B cell immunity, and T and B cell immunity according to their involvement in activation, proliferation, or differentiation of T cell and/or B cell. Graduation of genes in percentages is shown. *B*: mRNA expression levels for secreted phosphoprotein 1 (SPP1)/OPN in MAT and EAT and for CD4, CD8 α , and forkhead box protein P3 (Foxp3) in MAT are depicted. mRNA levels were determined by RT-qPCR (n = 7–12) and expressed as relative to C group. Data were analyzed by $\Delta\Delta C_q$ method and normalized to Actb, Gapdh, and Hprt1 gene expression. *C*: Western blot analysis of OPN, using protein extracts from MAT (n = 6) and an OPN-specific monoclonal antibody and as invariant control Actb. *D*: densitometric analysis of Western blot results is shown (n = 6). *E*: plasma OPN was quantified with commercially available ELISA kit (n = 7–11). All data are means \pm SE and were collected after 12 wk of feeding either C, HF, or HF/n-3. Statistical analysis was performed using 1-way ANOVA and Tukey posttest. *P < 0.05, **P < 0.01, ***P < 0.001, significant differences compared with control or between groups as indicated.

measured the mRNA expression of genes for the classical proinflammatory tumor necrosis factor- α (TNF α) and MCP-1 (8), the anti-inflammatory IL-10 (45), and the blood plasma levels of MCP-1 and SAA protein. Systemically increased SAA levels have been associated with obesity-associated diseases like insulin resistance and atherosclerosis (80). Figure 4 shows that mRNA levels for both TNF α and IL-10 were significantly upregulated in EAT from HF/n-3 mice compared with controls. In contrast, for MAT, TNF α and IL-10 mRNA levels were not changed (Fig. 4, *A* and *B*). For MCP-1, mRNA levels were significantly elevated in EAT

and MAT upon both high-fat diets, whereas MCP-1 levels were higher in EAT than in MAT. ELISA measurements of plasma MCP-1 concentrations showed only trends of slightly higher levels upon both high-fat diets than in controls (Fig. 4C). Importantly, plasma SAA levels were significantly elevated in HF mice as expected, whereas SAA levels were as low as controls upon HF/n-3 (Fig. 4D).

Differential expression of macrophage markers in MAT and EAT. Expansion of adipose tissues in obesity is associated with the accumulation of ATM. ATM can be identified by the macrophage marker F4/80 expression (2) and further classified

Table 4. Effects of LC-n-3 PUFA on expression of genes involved in immune cell activation in MAT

Fold Regulation HF vs. C Gene HF/n-3 vs. C HF/n-3 vs. HF Ap3b1 1.01 1.22 1.21 1.14 1.16 1.01 Bad Blr1 -1.111.13 1.24 Cb1b 1.10 1.79 1.63 Ccnd3 1.37 1.33 -1.03Cd1d1 1.55 1.33 -1.171.00 Cd2 -1.13-1.131.59 Cd28 -1.241.28 -149-127Cd3d -1.18Cd3e -1.321.02 1.35 Cd3 g 1.00 -1.06-1.06Cd4 -1.041.05 1.09 Cd40 1.38 1.57 1.14 Cd401 g -1.071.14 1.22 Cd74 1.22 1.36 1.11 Cd81 1.17 1.34 1.14 Cd8a -1.27-1.031.24 Cd8b1 -1.071.31 1 23 Cd93 1.38 1.58 1.14 Cdkn1a 2.51 1.71 -1.47Clcf1 -1.151.22 1.41 Cr2 -1.061.53 1.62 Csf2 -2.291.09 2.51 Cxcl12 1.04 1.72 1.65 Cxcr4 1.59 1.79 1.13 Dock2 -1.141.29 1.47 -1.051.33 1.40 Egr1 1.57 1.08 Flt3 1.46 Gadd45 g 1 57 1.09 -145Glmn 1.08 1.55 1.43 1.02 H2-Aa 1.21 1.18 Hdac5 1.11 -1.04-1.15Hdac7a 1.43 1.20 1.19 Hells -1.041.60 1.66 Hsp90aa1 1.62 1.71 1.05 Icosl 1.15 1.39 1.21 Ifng -6.301.19 7.49 1.01 -1.10Igbp1 1.11 II-10 -1.081.37 1.48 -1.90II12b -1.041.83 I115 -1.17-1.111.05 I118 -1.62-1.451.11 I127 1.18 1.27 1.08 Il2ra 1.28 2.46 1.93 2.22 I17 1.56 1.42 Impdh1 -1.14-1.041.10 Impdh2 -122-1.091.11 1.04 Inha -1.06-1.10Irf4 -1.041.45 1.51 3.11 4.59 1.48 Jag2 Ms4a1 -1.301.30 1.69 Nkx2-3 -1.20-1.161.03 Nos2 2.94 2.35 -1.25Pawr -1.03-1.05-1.02Pdcd1lg2 1.02 1.08 1.05 Pik3cd -1.15-1.011.14 PiK3r1 -1.10-1.10-1.00Prkcd 1.25 1.62 1.30 Prkcq -1.111.08 1.19 -1.50-1.09Prlr -1.64-1.161.26 1.46 Ptprc Relb 1.11 1.06 -1.05Rgs1 1.26 1.55 1.23 Sit1 -1.021.29 1.32 -1.02Sla2 1.16 1.13 Socs5 1.11 1.26 1.13

Table 4.—Continued

Gene	Fold Regulation					
	HF vs. C	HF/n-3 vs. C	HF/n-3 vs. HF			
Spp1	-1.61	9.45	15.19			
Tlr1	-1.08	1.58	1.71			
Tlr4	1.04	1.88	1.81			
Tlr6	-1.16	1.71	1.98			
Tnfrsf13b	-1.22	1.21	1.48			
Tnfrsf13c	2.70	3.05	1.13			
Tnfsf13b	1.42	1.88	1.32			
Tnfsf14	1.12	1.65	1.47			
Traf6	1.05	1.20	1.14			
Vav1	1.02	1.41	1.38			
Was	-1.11	1.20	1.33			
Wwp11	3.52	5.74	1.63			

Shown are the results for explorative gene expression analysis in MAT, using RT 2 Profiler RT-qPCR arrays (SABiosciences) for marker genes of T and B cell activation. mRNA expression levels are depicted as relative fold changes. An equal amount of RNA from 4 animals/dietary group was pooled, and 1 μg of pooled RNA was reverse transcribed and amplified according to the manufacturer's instructions. Data were normalized and analyzed with $\Delta\Delta C_q$ method, and fold changes were calculated relative to C or HF group. Targets with C_q values of ${\geq}35$ were excluded.

according to their state of activation/polarization into the proinflammatory M1 macrophages and anti-inflammatory M2 macrophages (20). The gene Emr1 (EGF-like module containing, mucin-like, hormone receptor-like sequence 1) encodes F4/80, and the genes integrin αX (Itgax) and mannose receptor C type 1 (Mrc1) are known to encode CD11c (marker for M1 macrophage subset) and CD206 (marker for M2 macrophage subsets), respectively (18).

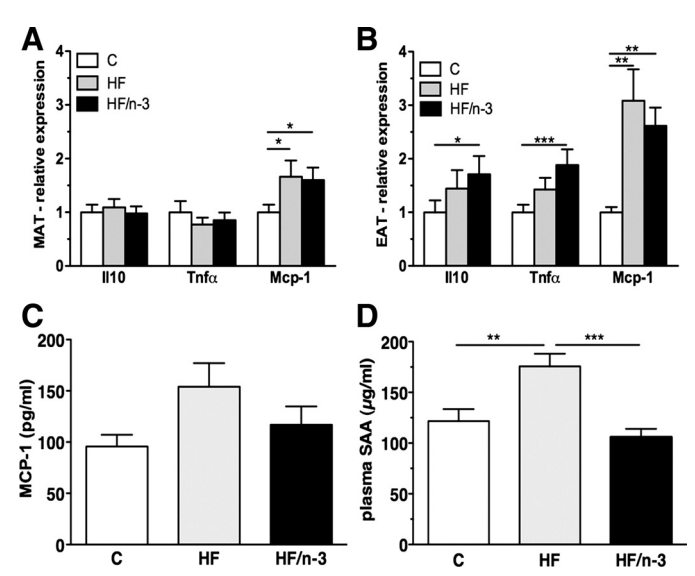


Fig. 4. Gene and protein expression of pro- and anti-inflammatory markers in VAT and plasma. All data are means \pm SE and were collected after 12 wk of feeding either C, HF, or HF/n-3. mRNA levels were measured for interleukin-10 (IL-10), tumor necrosis factor α (TNF α), and monocyte chemoattractant protein-1 (MCP-1) in MAT (A) and EAT (B) by RT-qPCR (n = 7-12) and expressed as relative to controls. Data were analyzed by $\Delta\Delta C_q$ method and normalized to β -actin, Gapdh, and Hpr11 gene expression. MCP-1 (C) and serum amyloid A (SAA) plasma levels (D) were quantified with commercially available ELISA kits. Statistical analysis was performed using 1-way ANOVA and Tukey posttest. *P < 0.05, **P < 0.01, and ***P < 0.001, significant differences compared with control or between groups as indicated.

RT-qPCR analyses revealed significantly increased Emr1 gene expression in EAT from HF/n-3 and HF animals compared with controls, whereas in MAT only significantly higher Emr1 mRNA levels were measured upon HF/n-3 than in controls (Fig. 5, A and B). Itgax mRNA expression was significantly elevated in EAT and MAT upon HF/n-3 compared with both HF and C diet, whereas Itgax expression was increased only in EAT upon HF. For HF/n-3 mice, mRNA expression of Itgax was much higher in EAT than in MAT. Similar gene expression changes were detected for another known macrophage marker, CD11b (integrin \alpha M; data not shown). For Mrc1 gene expression in MAT, a significant upregulation was measured upon HF/n-3 and HF compared with controls, but also a significant difference between the two high-fat diets was detected. In contrast, only a slight but significant difference was detected for Mrc1 mRNA levels in EAT upon HF/n-3 compared with the HF and C diet.

To assess the presence of macrophages in CLS in MAT and EAT, immunohistochemical analyses, using primary antibodies specific for F4/80, CD11c, and CD206 (Fig. 6), and quantification of the density of stained CLS were performed (Fig. 5, *C* and *D*). F4/80-positive CLS staining was almost zero in MAT from control animals (Figs. 5*C* and Fig. 6*A*), whereas F4/80-positive CLS were substantially more frequent in MAT upon HF/n-3 than upon HF (Fig. 5*C* and Fig. 6, *B* and *C*). Similarly, compared with controls, for HF and HF/n-3 mice, F4/80-positive CLS densities were significantly higher in EAT (Figs. 5*D* and 6, *D*–*F*). Notably, the F4/80-positive CLS

densities were about twofold higher in EAT than MAT upon HF/n-3 and even substantially 22.5-fold elevated upon HF (Fig. 5, C and D). CD11c-positive-stained CLS in MAT were significantly more abundant in HF/n-3 mice compared with HF and control mice (Figs. 5C and 6, G–I) as well as EAT from mice of all three dietary groups (Fig. 5, C and D, and 6, J–L). The density of CD11c-positive-stained CLS was only slightly higher in EAT than in MAT upon HF (Figs. 5, C and D, and 6, H and H). For the M2 macrophage marker CD206 (Figs. 5, H and H0, and 6, H1, we observed a significant elevation of positive CLS in MAT upon HF/n-3 compared with H2 and H3, whereas in EAT there was a trend only for higher CLS density upon both high-fat diets compared with controls (H2 = 0.0628).

LC-n-3 PUFA may mediate intestinal anti-inflammatory and splenic immunosuppressive effects. To get new insights into whether dietary LC-n-3 PUFA can induce endothelial gene expression changes in blood and lymphatic vessels of the small intestine in obese mice, we applied RT-qPCR array experiments in an explorative approach. The gene expression array analysis displayed that a significant fraction of genes were downregulated upon HF/n-3, especially in the HF/n-3 to HF comparison. Moreover, the majority of these genes were assigned to operate in endothelial cell activation, cell-cell or cell-matrix adhesion, and extracellular matrix remodeling (data not shown). For validation, we quantified the gene expression of target proteins that are involved in endothelial cell activation and growth or regulation of angiogenesis (39, 59), such as the classical adhesion molecules intercellular adhesion molecule 1

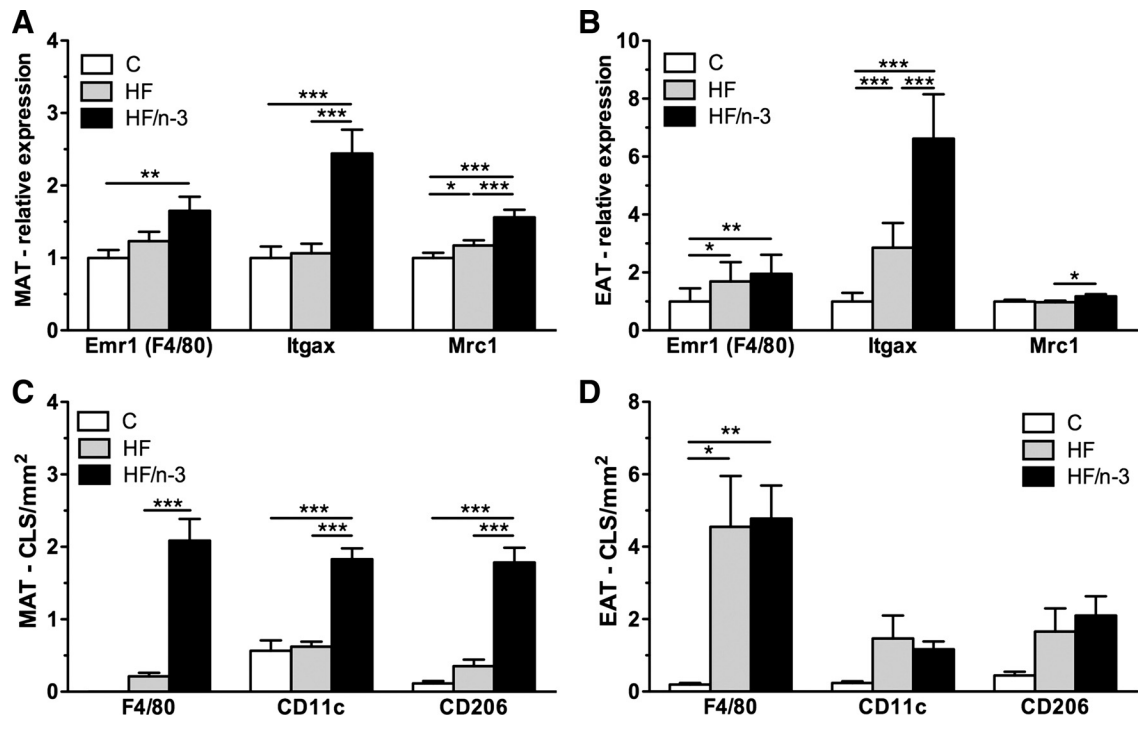


Fig. 5. Differential mRNA expression of genes encoding M1 and M2 macrophage markers and their immunohistochemical detection and quantification in crown-like structures (CLS) of VAT. All data are means \pm SE and were collected from MAT or EAT after 12 wk of feeding either C, HF, or HF/n-3. Gene expression data for Emr1 (F4/80), integrin α -X (Itgax; CD11c), and mannose receptor C type 1 (Mrc1; CD206) in MAT (A) and EAT (B) were retrieved by RT-qPCR (n=8-12) and calculated relative to controls. RT-qPCR data were analyzed by $\Delta\Delta$ Cq method and normalized to β -actin, Gapdh, and Hpr11 gene expression. C and D: quantitative analysis of CLS in tissue sections by immunohistochemistry, as shown in Fig. 6. No. of CLS stained positively for macrophage markers F4/80, CD11c, or CD206 in MAT (C) and EAT (D) expressed as CLS relative to mm² section area (n=4/group). Statistical analysis was performed using 1-way ANOVA and Tukey posttest. *P<0.05, **P<0.01, and ***P<0.001, significant differences compared with control or between groups as indicated.

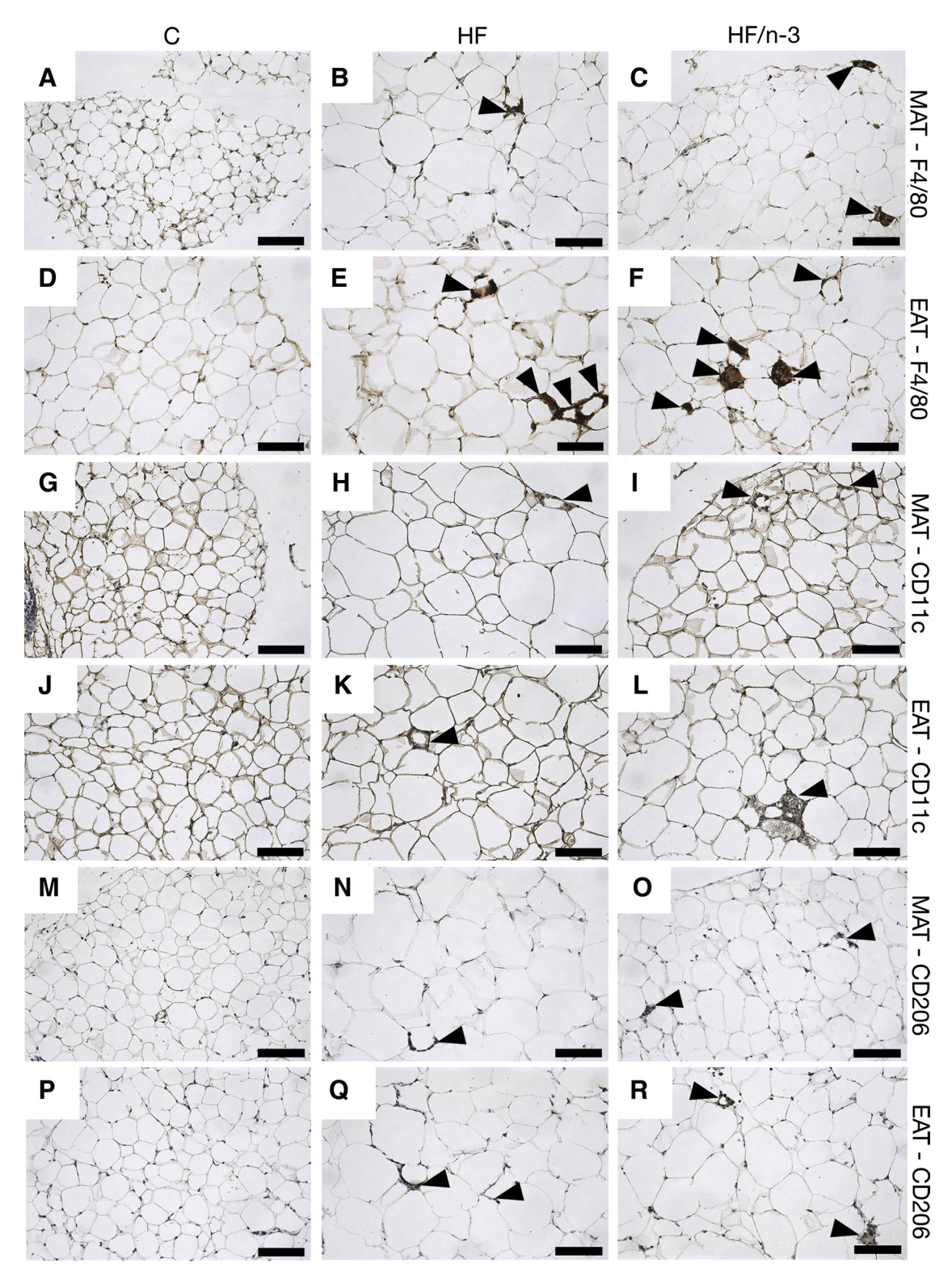


Fig. 6. Immunohistochemistal analysis of macrophage-associated M1 and M2 marker expression in CLS of MAT and EAT. Shown are paraformaldehyde-fixed paraffin sections of MAT and EAT from mice fed HF (B, E, H, K, N, and Q), HF/n-3 (C, F, I, L, O, and R), and control diet (A, D, G, J, M, and P) stained with primary antibodies specific for F4/80 (A-F), CD11c (G-L), or CD206 (M-R). For antigen signal detection, corresponding specific secondary antibodies combined with horseradish peroxidase-based detection system were applied, followed by counterstaining with hematoxylin. Arrowheads point to positive-stained cells in CLS surrounding adipocytes. Scale bar indicates 100 μ m.

(Icam1) and vascular cell adhesion molecule 1 (Vcam1) and endothelial-specific receptor tyrosine kinase (Tek). For mucosal tissue of the small intestine, Icam1 and Tek mRNA levels were significantly higher in HF mice than controls, and Vcam1 showed the same trend (Fig. 7A). Although statistical significance was not reached, the mRNA expression for Icam1, Vcam1, and Tek was lower upon HF/n-3, reaching levels similar to controls, compared with HF.

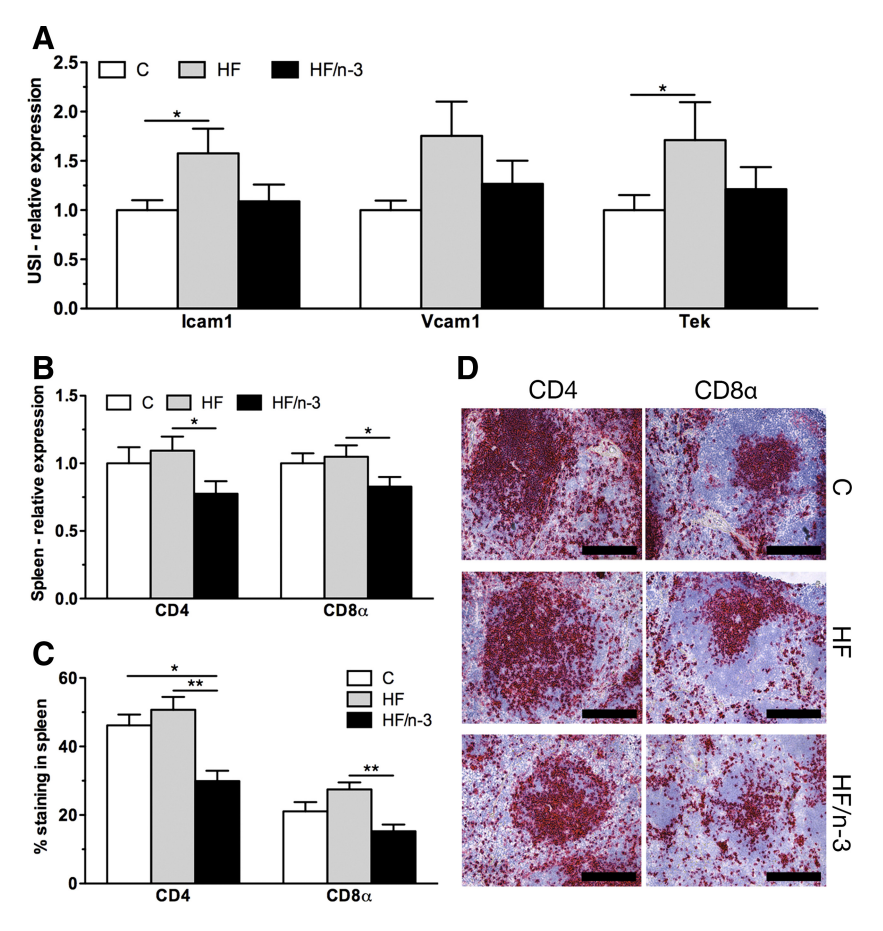
With regard to the significantly increased spleen mass in HF/n-3 mice (Table 3), this could have merely been an effect of body mass increase on high-fat diet. Therefore, we calculated spleen mass relative to body mass and still found, compared with controls, a significant increase in spleen mass upon HF/n-3, whereas spleen mass was decreased upon HF. Considering our results on immune cell activation in MLN containing MAT samples, we examined the spleen, which, like MLN, represents a secondary lymphoid organ and is a major site of lymphocyte proliferation and immune system homeostasis (43). Changes in the spleen were evaluated by measurements of splenic mRNA levels for CD4 and CD8α, with both identifying helper T lymphocytes and cytotoxic/suppressor T lymphocytes, respectively (12). Importantly, in contrast to HF and lean control mice, CD4 and CD8α gene expression was decreased significantly in HF/n-3 mice (Fig. 7B). These findings were confirmed by immunohistochemical analysis of spleen tissues and quantification of T cell marker-positivestained areas in the splenic white pulps, using primary antibodies specific for mouse T cell markers CD4 and CD8α (Fig. 7, C and D, and data not shown). These analyses revealed a significant reduction of positive-stained T cell areas in the splenic white pulps of HF/n-3 mice compared with HF and control mice.

DISCUSSION

In the present study, we have assessed whether metabolic and immunomodulatory processes are differentially modulated in MAT and EAT of C57BL/J mice fed defined soybean/palm oil-based control diet, HF diet, and LC-n-3 PUFA-enriched high-fat diet (HF/n-3) for 12 wk. Furthermore, we have examined metabolic and immunomodulatory processes in MATadjacent liver and intestine and iBAT and spleen to complement our findings on VAT in mice. Our study proved the protective role of dietary LC-n-3 PUFA on weight gain by reducing adipose tissue growth and demonstrated the lipidlowering effect on hepatic TAG and plasma NEFA levels, consistent with improved insulin levels and gene expression changes in liver and BAT. Most importantly, we identified a differential responsiveness to diets for VAT through preferentially metabolic alterations in MAT and inflammatory processes in EAT. The identified LC-n-3 PUFA effects were both pro- and anti-inflammatory and disclosed T cell-immunosuppressive potential. Moreover, our data indicate that LC-n-3 PUFA may alleviate high-fat diet-induced endothelial cell activation in the MAT-adjacent small intestine.

For fat mass-reducing LC-n-3 PUFA effects, we demonstrated that MAT adipocytes were more responsive to HF/n-3, as shown by their significantly smaller size compared with

Fig. 7. Gene expression analysis of the small intestine and CD4 and CD8 a mRNA expression and immunohistochemistry in spleen. All data are means ± SE and were collected after 12 wk of feeding either C, HF, or HF/n-3. A and B: shown are the gene expression for intercellular adhesion molecule 1 (Icam1), vascular cell adhesion molecule 1 (Vcam1), and endothelial tyrosine kinase (Tek) in small intestine (A) and for CD4 and CD8 α in spleen (B) measured by RT-qPCR (n = 8-12) and calculated relative to C group. RT-qPCR data were analyzed by $\Delta\Delta C_q$ method and normalized to β -actin, Gapdh, and Hprt1 gene expression. C: quantitative analysis of immunohistochemically CD4- and CD8α-positive-stained areas of splenic white pulps from mice of all 3 dietary groups (n =4-6). D: corresponding immunohistochemistry. Shown are representative digital images of CD4- and CD8-positivestained areas of the splenic white pulps taken from stained spleen cryosections. For immunohistochemistry, CD4- and CD8α-specific antibodies and antigen-detection system, including Fast Red, were used. Scale bar indicates 200 µm. Positive-stained areas are related to section area. Statistical analysis was performed using 1-way ANOVA and Tukey posttest. *P < 0.05 and **P < 0.01, significant differences compared with control or between groups as indicated.



EAT adipocytes. These findings may be a consequence of a higher metabolic activity of MAT compared with EAT due to its abdominal location being drained by the portal vein and higher blood flow, as shown in rats (78). Moreover, the observed higher correlation of leptin gene expression with body mass for MAT than EAT suggests that MAT mass may be a predictive marker for body mass/fat mass gain. Interestingly, LC-n-3 PUFA-mediated fat mass-reducing effects were observed in HF/n-3 mice, although HF/n-3 mice had a higher energy intake and a reduced fecal energy loss compared with HF mice. Additionally, neither indirect calorimetry nor locomotor analysis revealed any significant differences between high-fat diet-fed animals (data not shown). Importantly, the higher relative UCP1 expression capacity index for iBAT in HF/n-3 mice suggests an increased energy expenditure by uncoupling of the respiratory chain activity with elevated heat production upon LC-n-3 PUFA (3). In line with our data, Sadurskis et al. (58) demonstrated LC-PUFA-mediated upregulation of UCP gene expression.

Regarding the link of visceral obesity to reduced insulin sensitivity, we found a significant improvement in plasma insulin levels but only modest effects on glucose clearance in HF/n-3 mice. This may be partly a result of the observed reduced hepatic TAG concentrations and lower nonfasting plasma NEFA (29, 30, 42) in HF/n-3 mice, consistent with the downregulation of the lipogenic genes Scd-1 and Acaca (15, 28) and the upregulation of Acox1, which initiates peroxisomal β -oxidation, in the liver (13, 56). The observed unaltered hepatic Cpt1a expression indicates increased activity in peroxisomal β -oxidation and unchanged mitochondrial β -oxidation (15).

Excessive adipose tissue growth is associated with hypoxia, increased fat cell turnover, and a chronic low-grade proinflammatory state involving immune cell infiltration (55, 70). This is characterized by preceding T and B cells, followed by macrophage infiltration and polarization toward a more proinflammatory phenotype (18, 33, 47, 77, 79). In addition, the presence of various immune cells in CLS and the secretion of predominantly proinflammatory adipokines in expanded adipose tissues have been described (10, 21, 36). Proinflammatory processes in adipose tissues can be induced by factors like saturated fatty acids or n-6 PUFA, whereas LC-n-3 PUFA can counteract adipose tissue inflammation (4, 69). In the present study, the reduction of adipose tissue mass and the low levels of hepatic TAG and plasma NEFA and SAA in HF/n-3 compared with HF mice point to an amelioration of adipose tissue inflammation. In contrast, however, gene expression analyses displayed increased mRNA levels for genes involved in T and B cell activation in MAT upon HF/n-3 compared with HF. OPN was especially found to be highly upregulated in MAT and EAT. OPN is one of the most abundant proteins synthetized by activated T lymphocytes (76) and is expressed in EAT of obese mice (31). Furthermore, OPN mediates obesity-induced macrophage infiltration into adipose tissue and insulin resistance in mice (48). Therefore, the observed high levels for OPN in MAT and EAT from HF/n-3 mice could be derived from T cells and/or adipocytes. It is important to note that MAT includes MLN, which are involved in immune response, whereas EAT does not contain lymph nodes (32, 52). MLN can enlarge due to the expansion of MLN immune cells upon immune responses of the body. In this study, we have not observed obviously enlarged MLN in mice, and therefore, the

naturally tiny MLN were intentionally not dissected out from analyzed MAT of all three dietary groups. Thus, we cannot rule out that our data on T cell- and B cell-specific gene expression in MAT may be more reflective of immune cells in lymph nodes than of proper MAT. The marked increase in OPN levels pointed to T cell activation-induced proliferation. However, reduced CD8α mRNA levels and diminished CD4 and Foxp3 mRNA levels in MAT from HF/n-3 mice indicated a reduction in T cells. As an underlying mechanism, we propose T cell activation-induced apoptosis in MAT and preferentially in MLN, which was induced by increased DHA and EPA content in the diet. Our assumption is based on studies by Mattacks et al. (41) and Pond and Mattacks (53) concluding that perinodal adipocytes provide immune cells with essential fatty acids that may stimulate or attenuate the activation of immune cells. Notably, in that context, Kim et al. (32) reported that in obese mice visceral fat accumulation causes atrophy of MLN by enhanced activation-induced T cell apoptosis in MLN, implicating dietary fat-induced visceral obesity in obesity-related immune dysfunction. Importantly, we found that HF/n-3 also had a T cell-reducing effect on the spleen, which is a secondary lymphoid organ, as are MLN. The reduced CD4- and CD8αpositive T cells in the splenic white pulps of HF/n-3 mice may indicate changes in immune activation, as reported in other studies with fish oil feeding (40), although obvious pathological changes were not observed. With regard to increased spleen mass of HF/n-3 mice, this could reflect a physiological adaptation to higher erythrocyte turnover, as reported by Oarada et al. (49). Considering the potential suppressive effects of dietary LC-n-3 PUFA on protective components of T cellmediated inflammatory response in MLN and spleen in mice, future experiments are warrantable to explore specifically how dietary LC-n-3 PUFA may affect the immune response in mice upon different immune challenges.

Regarding the inflammatory processes in expanding adipose tissues, ATM are a prominent source of IL-6 and TNF α , providing a causal link between macrophage infiltration and activation and adipose tissue inflammation in obesity and insulin resistance (77). This is often associated with a switch in polarization of ATM from an anti-inflammatory M2 state to a proinflammatory M1 state (37, 38), possibly caused by processes involving macrophage lipotoxity (54). M1 macrophages accumulate preferentially around dead adipocytes, thereby forming necrotic CLS, whereas M2 macrophages are associated with adipose tissue remodeling and repair processes (10, 38). The mRNA upregulation for proinflammatory TNF α and anti-inflammatory IL-10 upon HF/n-3 in EAT but not in MAT suggests that LC-n-3 PUFA increased a proinflammatory state preferentially in EAT. Interestingly, the presence of MLN in our analyzed MAT samples apparently did not lead to MLNdriven high levels of cytokines in obese mice, as judged by rather moderate mRNA expression patterns for TNF α and IL-10 in MAT in all dietary groups compared with EAT. With regard to ATM infiltration, the gene expression of the macrophage markers F4/80, CD11c, and CD206 and their immunohistological CLS localization in VAT demonstrate a stronger infiltration of macrophages in EAT than in MAT from mice fed high-fat diets. This is consistent with the observed more proinflammatory state in EAT than in MAT and with the increased MCP-1 mRNA levels in VAT upon both high-fat diets. In addition, the high CD11c expression in EAT from HF/n-3 mice could indicate that ATM are predominantly of the classical activated M1 state (54) and/or that the number of other dendritic immune cells belonging to the cell family of mononuclear phagocytes (27) increased simultaneously. This consideration may apply partly to MAT from obese HF/n-3 mice. However, the elevated expression of the M2 macrophage marker CD206 in MAT upon HF/n-3 indicates the presence of M2 macrophages. Taken together, our data suggest that the polarization status of ATM in EAT and MAT may have switched toward a more pro- or anti-inflammatory state depending on the quality of fatty acids such as LC-n-6 PUFA and LC-n-3 PUFA and/or their conversion to corresponding metabolites such as eicosanoids and resolvins E1 and D1, respectively (25, 68). For more detailed analyses of ATM, fluorescence-activated cell sorter-based analysis of isolated immune cells from VAT and immunofluorescence microscopy of double- and triple-immunostained tissue sections are necessary. However, these analyses were not in the scope of our study.

In HF/n-3 mice, the known anti-inflammatory properties for dietary LC-n-3 PUFA were supported by our findings on reduced SAA plasma levels (61, 80), increased M2 macrophage marker expression in MAT, and indicatively alleviated HF-induced endothelial cell activation and regulation of angiogenesis in the small intestine. In contrast, LC-n-3 PUFA effects confined to EAT exhibited a predominantly proinflammatory gene expression signature, and the T cell reduction in splenic white pulps of HF/n-3 mice disclose immunosuppressive effects. These observed differences regarding changes in inflammatory state challenge the current perception that LCn-3 PUFA act solely anti-inflammatory (26, 69). However, these apparently opposing LC-n-3 PUFA effects may also be a consequence of different background diets applied. Palm oil was used as the main fat for the high-fat diets in our study because it is a major ingredient in human diets with proven adverse health effects (72) and has a high content of saturated fat (35.81%). The role of saturated fatty acids in promoting diet-dependent diseases and inflammation has been studied extensively, but much less is known about possible proinflammatory actions of LC-n-3 PUFA. For example, it has been reported that dietary supplementation with EPA and DHA can increase TNF α and IL-6 production in peritoneal macrophages (66) and other cell types through downregulation of prostaglandin E₂ (65). These cytokines can increase lipolysis and suppress preadipocyte differentiation (50, 81), and thereby preadipocytes may increase their potency for proinflammatory gene expression and macrophage recruitment (39). However, contrary effects involving NF-κB- and PPARγdependent mechanisms have also been observed (34). Thus, pro- and anti-inflammatory effects of LC-n-3 PUFA can occur at the same time (65) and may vary widely depending on the cell type (75) and study conditions (17), such as treatment duration and the use of different high-fat diets, which can be based on either rapeseed/sunflower oil (57), safflower oil/lard (69), or palm oil (11).

Considering our observed LC-n-3 PUFA effects on MAT in obese mice and the potential cross-talk of MAT with the liver and intestine, it is tempting to speculate that *I*) the increase in LC-n-3 PUFA in cell membranes and/or the generation of their lipid mediators resulted in improved intestinal epithelial tissue homeostasis and vascular endothelial cell function, 2) LC-n-3 PUFA-induced T cell activation diminished the responsiveness

to T cell proliferation but increased vulnerability to apoptosis, especially in CD8-positive T cells in MLN and spleen, and 3) LC-n-3 PUFA increased the inflammatory state in EAT but lowered macrophage lipotoxity, possibly preferentially in MAT, resembling more a physiological state of inflammation, which is compatible with lower fat mass and improved lipid metabolism in contrast to the pathological state of inflammation.

Taken together, this study demonstrates that in a DIO mouse model dietary LC-n-3 PUFA DHA and EPA exert antiobesogenic effects and apparently improve the overall health status of obese mice, as judged by reduced hepatic TAG accumulation and lower plasma NEFA concentrations as well as improved plasma insulin levels. Most importantly, our data revealed differential responsiveness to diets for VAT through preferentially metabolic alterations for MAT and inflammatory processes for EAT. Furthermore, the observed immunomodulatory LC-n-3 PUFA effects displayed pro- and anti-inflammatory characteristics and T cell-immunosuppressive potential, suggesting that a LC-n-3 PUFA-enriched diet with a balanced n-6/n-3 PUFA ratio can exert both immune-enhancing and -suppressive effects in different tissues and/or cell types. In future studies, it will be of interest to test whether dietary LC-n-3 PUFA supplementation may have differing effects in nonobese and obese mice and relative to sex and similarly in healthy subjects compared with metabolic syndrome patients.

ACKNOWLEDGMENTS

We thank Christoph Dahlhoff, Dominika Kolodziejczak, and Ronny Scheundel for their technical assistance and help during tissue sampling, and we appreciate the technical assistance of Ruth Hillermann for immunohistochemical analyses.

GRANTS

This work and T. Ludwig and S. Worsch were supported by the German Research Foundation as part of the Research Training School GRK 1482. M. Heikenwalder was supported by the Helmholtz Foundation and a Starting Grant (LiverCancerMechanism) from the European Research Council.

DISCLOSURES

The authors have no conflicts of interest, financial or otherwise, to declare.

AUTHOR CONTRIBUTIONS

T.L., H.D., H.H., and B.L.B. contributed to the conception and design of the research; T.L. and S.W. performed the experiments; T.L., S.W., M.H., and B.L.B. analyzed the data; T.L., M.H., and B.L.B. interpreted the results of the experiments; T.L. and S.W. prepared the figures; T.L. and B.L.B. drafted the manuscript; T.L., S.W., M.H., H.D., H.H., and B.L.B. approved the final version of the manuscript; B.L.B. edited and revised the manuscript.

REFERENCES

- Ailhaud G, Guesnet P. Fatty acid composition of fats is an early determinant of childhood obesity: a short review and an opinion. *Obes Rev* 5: 21–26, 2004.
- Austyn JM, Gordon S. F4/80, a monoclonal antibody directed specifically against the mouse macrophage. Eur J Immunol 11: 805–815, 1981.
- Beck V, Jaburek M, Demina T, Rupprecht A, Porter RK, Jezek P, Pohl EE. Polyunsaturated fatty acids activate human uncoupling proteins 1 and 2 in planar lipid bilayers. FASEB J 21: 1137–1144, 2007.
- Buettner R, Parhofer KG, Woenckhaus M, Wrede CE, Kunz-Schughart LA, Schölmerich J, Bollheimer LC. Defining high-fat-diet rat models: metabolic and molecular effects of different fat types. *J Mol Endocrinol* 36: 485–501, 2006.
- Caesar R, Manieri M, Kelder T, Boekschoten M, Evelo C, Müller M, Kooistra T, Cinti S, Kleemann R, Drevon CA. A combined transcriptomics and lipidomics analysis of subcutaneous, epididymal and mesen-

- teric adipose tissue reveals marked functional differences. *PLoS One* 5: e11525, 2010.
- Calle EE, Rodriguez C, Walker-Thurmond K, Thun MJ. Overweight, obesity, and mortality from cancer in a prospectively studied cohort of U.S. adults. N Engl J Med 348: 1625–1638, 2003.
- Catalano KJ, Stefanovski D, Bergman RN. Critical role of the mesenteric depot versus other intra-abdominal adipose depots in the development of insulin resistance in young rats. *Diabetes* 59: 1416–1423, 2010.
- Chen A, Mumick S, Zhang C, Lamb J, Dai H, Weingarth D, Mudgett J, Chen H, MacNeil DJ, Reitman ML, Qian S. Diet induction of monocyte chemoattractant protein-1 and its impact on obesity. *Obes Res* 13: 1311–1320, 2005.
- Chen HC, Farese RV Jr. Determination of adipocyte size by computer image analysis. J Lipid Res 43: 986–989, 2002.
- Cinti S, Mitchell G, Barbatelli G, Murano I, Ceresi E, Faloia E, Wang S, Fortier M, Greenberg AS, Obin MS. Adipocyte death defines macrophage localization and function in adipose tissue of obese mice and humans. *J Lipid Res* 46: 2347–2355, 2005.
- 11. de Wit NJ, Boekschoten MV, Bachmair EM, Hooiveld GJ, de Groot PJ, Rubio-Aliaga I, Daniel H, Müller M. Dose-dependent effects of dietary fat on development of obesity in relation to intestinal differential gene expression in C57BL/6J mice. *PLoS One* 6: e19145, 2010.
- Ellmeier W, Sawada S, Littman DR. The regulation of CD4 and CD8 coreceptor gene expression during T cell development. *Annu Rev Immunol* 17: 523–554, 1999.
- 13. Fan CY, Pan J, Chu R, Lee D, Kluckman KD, Usuda N, Singh I, Yeldandi AV, Rao MS, Maeda N, Reddy JK. Hepatocellular and hepatic peroxisomal alterations in mice with a disrupted peroxisomal fatty acylcoenzyme A oxidase gene. *J Biol Chem* 271: 24698–24710, 1996.
- Fedor D, Kelley DS. Prevention of insulin resistance by n-3 polyunsaturated fatty acids. Curr Opin Clin Nutr Metab Care 12: 138–146, 2009.
- Flachs P, Horakova O, Brauner P, Rossmeisl M, Pecina P, Franssenvan Hal N, Ruzickova J, Sponarova J, Drahota Z, Vlcek C, Keijer J, Houstek J, Kopecky J. Polyunsaturated fatty acids of marine origin upregulate mitochondrial biogenesis and induce beta-oxidation in white fat. *Diabetologia* 48: 2365–2375, 2005.
- Foster MT, Shi H, Seeley RJ, Woods SC. Removal of intra-abdominal visceral adipose tissue improves glucose tolerance in rats: role of hepatic triglyceride storage. *Physiol Behav* 104: 845–854, 2011.
- Fritsche K. Important differences exist in the dose-response relationship between diet and immune cell fatty acids in humans and rodents. *Lipids* 42: 961–979, 2007.
- 18. Fujisaka S, Usui I, Bukhari A, Ikutani M, Oya T, Kanatani Y, Tsuneyama K, Nagai Y, Takatsu K, Urakaze M, Kobayashi M, Tobe K. Regulatory mechanisms for adipose tissue M1 and M2 macrophages in diet-induced obese mice. *Diabetes* 58: 2574–2582, 2009.
- 19. Gómez-Ambrosi J, Catalán V, Ramírez B, Rodríguez A, Colina I, Silva C, Rotellar F, Mugueta C, Gil MJ, Cienfuegos JA, Salvador J, Frühbeck G. Plasma osteopontin levels and expression in adipose tissue are increased in obesity. *J Clin Endocrinol Metab* 92: 3719–3727, 2007.
- Gordon S, Martinez FO. Alternative activation of macrophages: mechanism and functions. *Immunity* 32: 593–604, 2010.
- Guo KY, Halo P, Leibel RL, Zhang Y. Effects of obesity on the relationship of leptin mRNA expression and adipocyte size in anatomically distinct fat depots in mice. Am J Physiol Regul Integr Comp Physiol 287: R112–R119, 2004.
- Hariri N, Thibault L. High-fat diet-induced obesity in animal models. Nutr Res Rev 23: 270–299, 2010.
- 23. Harris RB, Leibel RL. Location, location, location... Cell Metab 7: 359-361, 2008.
- Hauner H. Secretory factors from human adipose tissue and their functional role. Proc Nutr Soc 64: 163–169, 2005.
- Hellmann J, Tang Y, Kosuri M, Bhatnagar A, Spite M. Resolvin D1 decreases adipose tissue macrophage accumulation and improves insulin sensitivity in obese-diabetic mice. FASEB J 25: 2399–2407, 2011.
- 26. Huber J, Löffler M, Bilban M, Reimers M, Kadl A, Todoric J, Zeyda M, Geyeregger R, Schreiner M, Weichhart T, Leitinger N, Waldhäusl W, Stulnig TM. Prevention of high-fat diet-induced adipose tissue remodeling in obese diabetic mice by n-3 polyunsaturated fatty acids. *Int J Obes (Lond)* 31: 1004–1013, 2007.
- Hume DA. Macrophages as APC and the dendritic cell myth. J Immunol 181: 5829–5835, 2008.

- Ide T. Interaction of fish oil and conjugated linoleic acid in affecting hepatic activity of lipogenic enzymes and gene expression in liver and adipose tissue. *Diabetes* 54: 412–423, 2005.
- 29. Jelenik T, Rossmeisl M, Kuda O, Jilkova ZM, Medrikova D, Kus V, Hensler M, Janovska P, Miksik I, Baranowski M, Gorski J, Hebrard S, Jensen TE, Flachs P, Hawley S, Viollet B, Kopecky J. AMP-activated protein kinase alpha2 subunit is required for the preservation of hepatic insulin sensitivity by n-3 polyunsaturated fatty acids. *Diabetes* 59: 2737– 2746, 2010.
- Kajikawa S, Harada T, Kawashima A, Imada K, Mizuguchi K. Highly purified eicosapentaenoic acid prevents the progression of hepatic steatosis by repressing monounsaturated fatty acid synthesis in high-fat/high-sucrose diet-fed mice. *Prostaglandins Leukot Essent Fatty Acids* 80: 229– 238, 2009.
- Kiefer FW, Zeyda M, Todoric J, Huber J, Geyeregger R, Weichhart T, Aszmann O, Ludvik B, Silberhumer GR, Prager G, Stulnig TM. Osteopontin expression in human and murine obesity: extensive local upregulation in adipose tissue but minimal systemic alterations. *Endocri*nology 149: 1350–1357, 2008.
- 32. Kim CS, Lee SC, Kim YM, Kim BS, Choi HS, Kawada T, Kwon BS, Yu R. Visceral fat accumulation induced by a high-fat diet causes the atrophy of mesenteric lymph nodes in obese mice. *Obesity (Silver Spring)* 16: 1261–1269, 2008.
- 33. Kintscher U, Hartge M, Hess K, Foryst-Ludwig A, Clemenz M, Wabitsch M, Fischer-Posovszky P, Barth TF, Dragun D, Skurk T, Hauner H, Blüher M, Unger T, Wolf AM, Knippschild U, Hombach V, Marx N. T-lymphocyte infiltration in visceral adipose tissue: a primary event in adipose tissue inflammation and the development of obesity-mediated insulin resistance. Arterioscler Thromb Vasc Biol 28: 1304–1310. 2008.
- 34. Li H, Ruan XZ, Powis SH, Fernando R, Mon WY, Wheeler DC, Moorhead JF, Varghese Z. EPA and DHA reduce LPS-induced inflammation responses in HK-2 cells: evidence for a PPAR-gamma-dependent mechanism. *Kidney Int* 67: 867–874, 2005.
- 35. **Livak KJ, Schmittgen TD.** Analysis of relative gene expression data using real-time quantitative PCR and the 2(-Delta Delta C(T)) Method. *Methods* 25: 402–408, 2001.
- Loffreda S, Yang SQ, Lin HZ, Karp CL, Brengman ML, Wang DJ, Klein AS, Bulkley GB, Bao C, Noble PW, Lane MD, Diehl AM. Leptin regulates proinflammatory immune responses. FASEB J 12: 57–65, 1998.
- Lumeng CN, Bodzin JL, Saltiel AR. Obesity induces a phenotypic switch in adipose tissue macrophage polarization. *J Clin Invest* 117: 175–184, 2007.
- Lumeng CN, DelProposto JB, Westcott DJ, Saltiel AR. Phenotypic switching of adipose tissue macrophages with obesity is generated by spatiotemporal differences in macrophage subtypes. *Diabetes* 57: 3239– 3246, 2008.
- 39. Mack I, BelAiba RS, Djordjevic T, Görlach A, Hauner H, Bader BL. Functional analyses reveal the greater potency of preadipocytes compared with adipocytes as endothelial cell activator under normoxia, hypoxia, and TNFα exposure. Am J Physiol Endocrinol Metab 297: E735–E748, 2009.
- Matsuzawa Y, Shimomura I, Nakamura T, Keno Y, Tokunaga K. Pathophysiology and pathogenesis of visceral fat obesity. *Ann NY Acad Sci* 748: 399–406, 1995.
- 41. Mattacks CA, Sadler D, Pond CM. Site-specific differences in fatty acid composition of dendritic cells and associated adipose tissue in popliteal depot, mesentery, and omentum and their modulation by chronic inflammation and dietary lipids. *Lymphat Res Biol* 2: 107–129, 2004.
- McKenney JM, Sica D. Role of prescription omega-3 fatty acids in the treatment of hypertriglyceridemia. *Pharmacotherapy* 27: 715–728, 2007.
- 43. **Mebius RE, Kraal G.** Structure and function of the spleen. *Nat Rev Immunol* 5: 606–616, 2005.
- Milne CD, Paige CJ. IL-7: a key regulator of B lymphopoiesis. Semin Immunol 18: 20–30, 2006.
- Murray PJ. The primary mechanism of the IL-10-regulated antiinflammatory response is to selectively inhibit transcription. *Proc Natl Acad Sci* USA 102: 8686–8691, 2005.
- Murray PJ, Wynn TA. Protective and pathogenic functions of macrophage subsets. *Nat Rev Immunol* 11: 723–737, 2011.
- 47. Nishimura S, Manabe I, Nagasaki M, Eto K, Yamashita H, Ohsugi M, Otsu M, Hara K, Ueki K, Sugiura S, Yoshimura K, Kadowaki T, Nagai R. CD8+ effector T cells contribute to macrophage recruitment and adipose tissue inflammation in obesity. *Nat Med* 15: 914–920, 2009.

- 48. Nomiyama T, Perez-Tilve D, Ogawa D, Gizard F, Zhao Y, Heywood EB, Jones KL, Kawamori R, Cassis LA, Tschöp MH, Bruemmer D. Osteopontin mediates obesity-induced adipose tissue macrophage infiltration and insulin resistance in mice. *J Clin Invest* 117: 2877–2888, 2007.
- Oarada M, Furukawa H, Majima T, Miyazawa T. Fish oil diet affects on oxidative senescence of red blood cells linked to degeneration of spleen cells in mice. *Biochim Biophys Acta* 1487: 1–14, 2000.
- Petruschke T, Hauner H. Tumor necrosis factor-alpha prevents the differentiation of human adipocyte precursor cells and causes delipidation of newly developed fat cells. J Clin Endocrinol Metab 76: 742–747, 1993.
- 51. Peyrin-Biroulet L, Chamaillard M, Gonzalez F, Beclin E, Decourcelle C, Antunes L, Gay J, Neut C, Colombel JF, Desreumaux P. Mesenteric fat in Crohn's disease: a pathogenetic hallmark or an innocent bystander? *Gut* 56: 577–583, 2007.
- Pond CM. Adipose tissue and the immune system. Prostaglandins Leukot Essent Fatty Acids 73: 17–30, 2005.
- Pond CM, Mattacks CA. The source of fatty acids incorporated into proliferating lymphoid cells in immune-stimulated lymph nodes. *Br J Nutr* 89: 375–383, 2003.
- 54. Prieur X, Mok CY, Velagapudi VR, Núñez V, Fuentes L, Montaner D, Ishikawa K, Camacho A, Barbarroja N, O'Rahilly S, Sethi JK, Dopazo J, Orešič M, Ricote M, Vidal-Puig A. Differential lipid partitioning between adipocytes and tissue macrophages modulates macrophage lipotoxicity and M2/M1 polarization in obese mice. *Diabetes* 60: 797–809, 2011.
- 55. Rausch ME, Weisberg S, Vardhana P, Tortoriello DV. Obesity in C57BL/6J mice is characterized by adipose tissue hypoxia and cytotoxic T-cell infiltration. *Int J Obes (Lond)* 32: 451–463, 2008.
- 56. Rustan AC, Christiansen EN, Drevon CA. Serum lipids, hepatic glycerolipid metabolism and peroxisomal fatty acid oxidation in rats fed omega-3 and omega-6 fatty acids. *Biochem J* 283: 333–339, 1992.
- 57. Ruzickova J, Rossmeisl M, Prazak T, Flachs P, Sponarova J, Veck M, Tvrzicka E, Bryhn M, Kopecky J. Omega-3 PUFA of marine origin limit diet-induced obesity in mice by reducing cellularity of adipose tissue. *Lipids* 39: 1177–1185, 2004.
- Sadurskis A, Dicker A, Cannon B, Nedergaard J. Polyunsaturated fatty acids recruit brown adipose tissue: increased UCP content and NST capacity. Am J Physiol Endocrinol Metab 269: E351–E360, 1995.
- 59. Sato TN, Tozawa Y, Deutsch U, Wolburg-Buchholz K, Fujiwara Y, Gendron-Maguire M, Gridley T, Wolburg H, Risau W, Qin Y. Distinct roles of the receptor tyrosine kinases Tie-1 and Tie-2 in blood vessel formation. *Nature* 376: 70–74, 1995.
- Schaffler A, Scholmerich J, Buchler C. Mechanisms of disease: adipocytokines and visceral adipose tissue—emerging role in intestinal and mesenteric diseases. *Nat Clin Pract Gastroenterol Hepatol* 2: 103–111, 2005.
- 61. Scheja L, Heese B, Zitzer H, Michael MD, Siesky AM, Pospisil H, Beisiegel U, Seedorf K. Acute-phase serum amyloid A as a marker of insulin resistance in mice. *Exp Diabetes Res* 2008: 230837, 2008.
- Serhan CN, Chiang N, Van Dyke TE. Resolving inflammation: dual anti-inflammatory and pro-resolution lipid mediators. *Nat Rev Immunol* 8: 349–361, 2008.
- 63. Simopoulos AP. The importance of the omega-6/omega-3 fatty acid ratio in cardiovascular disease and other chronic diseases. Exp Biol Med (Maywood) 233: 674–688, 2008.
- 64. Stulnig TM, Huber J, Leitinger N, Imre EM, Angelisova P, Nowotny P, Waldhausl W. Polyunsaturated eicosapentaenoic acid displaces proteins from membrane rafts by altering raft lipid composition. *J Biol Chem* 276: 37335–37340, 2001.
- Tai CC, Ding ST. N-3 polyunsaturated fatty acids regulate lipid metabolism through several inflammation mediators: mechanisms and implications for obesity prevention. *J Nutr Biochem* 21: 357–363, 2010.

- 66. Tappia PS, Man WJ, Grimble RF. Influence of unsaturated fatty acids on the production of tumour necrosis factor and interleukin-6 by rat peritoneal macrophages. *Mol Cell Biochem* 143: 89–98, 1995.
- Tilg H, Moschen AR. Adipocytokines: mediators linking adipose tissue, inflammation and immunity. Nat Rev Immunol 6: 772–783, 2006.
- 68. Titos E, Rius B, González-Périz A, López-Vicario C, Morán-Salvador E, Martínez-Clemente M, Arroyo V, Clària J. Resolvin D1 and its precursor docosahexaenoic acid promote resolution of adipose tissue inflammation by eliciting macrophage polarization toward an M2-like phenotype. *J Immunol* 187: 5408–5418, 2011.
- 69. Todoric J, Loffler M, Huber J, Bilban M, Reimers M, Kadl A, Zeyda M, Waldhausl W, Stulnig TM. Adipose tissue inflammation induced by high-fat diet in obese diabetic mice is prevented by n-3 polyunsaturated fatty acids. *Diabetologia* 49: 2109–2119, 2006.
- Trayhurn P, Wang B, Wood IS. Hypoxia in adipose tissue: a basis for the dysregulation of tissue function in obesity? Br J Nutr 100: 227–235, 2008
- 71. Van de Walle I, De Smet G, Gärtner M, De Smedt M, Waegemans E, Vandekerckhove B, Leclercq G, Plum J, Aster JC, Bernstein ID, Guidos CJ, Kyewski B, Taghon T. Jagged2 acts as a Delta-like Notch ligand during early hematopoietic cell fate decisions. *Blood* 117: 4449–4459, 2011.
- 72. Vega-López S, Ausman LM, Jalbert SM, Erkkilä AT, Lichtenstein AH. Palm and partially hydrogenated soybean oils adversely alter lipoprotein profiles compared with soybean and canola oils in moderately hyperlipidemic subjects. Am J Clin Nutr 84: 54–62, 2006.
- Vine DF, Charman SA, Gibson PR, Sinclair AJ, Porter CJ. Effect of dietary fatty acids on the intestinal permeability of marker drug compounds in excised rat jejunum. J Pharm Pharmacol 54: 809–819, 2002.
- Wajchenberg BL. Subcutaneous and visceral adipose tissue: their relation to the metabolic syndrome. *Endocr Rev* 21: 697–738, 2000.
- Wallace FA, Miles EA, Calder PC. Activation state alters the effect of dietary fatty acids on pro-inflammatory mediator production by murine macrophages. *Cytokine* 12: 1374–1379, 2000.
- Weber GF, Cantor H. The immunology of Eta-1/osteopontin. Cytokine Growth Factor Rev 7: 241–248, 1996.
- Weisberg SP, McCann D, Desai M, Rosenbaum M, Leibel RL, Ferrante AW Jr. Obesity is associated with macrophage accumulation in adipose tissue. *J Clin Invest* 112: 1796–1808, 2003.
- West DB, Prinz WA, Greenwood MR. Regional changes in adipose tissue blood flow and metabolism in rats after a meal. Am J Physiol Regul Integr Comp Physiol 257: R711–R716, 1989.
- 79. Winer DA, Winer S, Shen L, Wadia PP, Yantha J, Paltser G, Tsui H, Wu P, Davidson MG, Alonso MN, Leong HX, Glassford A, Caimol M, Kenkel JA, Tedder TF, McLaughlin T, Miklos DB, Dosch HM, Engleman EG. B cells promote insulin resistance through modulation of T cells and production of pathogenic IgG antibodies. *Nat Med* 17: 610–617, 2011.
- 80. Yang RZ, Lee MJ, Hu H, Pollin TI, Ryan AS, Nicklas BJ, Snitker S, Horenstein RB, Hull K, Goldberg NH, Goldberg AP, Shuldiner AR, Fried SK, Gong DW. Acute-phase serum amyloid A: an inflammatory adipokine and potential link between obesity and its metabolic complications. PLoS Med 3: e287, 2006.
- Zhang HH, Halbleib M, Ahmad F, Manganiello VC, Greenberg AS. Tumor necrosis factor-alpha stimulates lipolysis in differentiated human adipocytes through activation of extracellular signal-related kinase and elevation of intracellular cAMP. *Diabetes* 51: 2929–2935, 2002.
- Zhang X, Srinivasan SV, Lingrel JB. WWP1-dependent ubiquitination and degradation of the lung Kruppel-like factor, KLF2. *Biochem Biophys Res Commun* 316: 139–148, 2004.